

Chapman University

Chapman University Digital Commons

Pharmaceutical Sciences (MS) Theses

Dissertations and Theses


Fall 12-2023

Analyzing Functional Interactions of Designed Peptides by NMR Spectroscopy

Wonsuk Choi

Chapman University, wonchoi@chapman.edu

Follow this and additional works at: https://digitalcommons.chapman.edu/pharmaceutical_sciences_theses

 Part of the [Medicinal and Pharmaceutical Chemistry Commons](#), [Other Biochemistry, Biophysics, and Structural Biology Commons](#), [Other Pharmacy and Pharmaceutical Sciences Commons](#), [Pharmaceutical Preparations Commons](#), [Pharmaceutics and Drug Design Commons](#), and the [Structural Biology Commons](#)

Recommended Citation

Choi, W. *Analyzing Functional Interactions of Designed Peptides by NMR Spectroscopy*. [master's thesis]. Irvine, CA: Chapman University; 2023. <https://doi.org/10.36837/chapman.000507>

This Thesis is brought to you for free and open access by the Dissertations and Theses at Chapman University Digital Commons. It has been accepted for inclusion in Pharmaceutical Sciences (MS) Theses by an authorized administrator of Chapman University Digital Commons. For more information, please contact laughtin@chapman.edu.

Analyzing Functional Interactions of Designed Peptides by NMR Spectroscopy

A Thesis by

Wonsuk Choi

Chapman University

Irvine, CA

School of Pharmacy

Submitted in partial fulfillment of the requirements for the degree of

Master of Science in Pharmaceutical Sciences

December 2023

Committee in charge:

Innokentiy Maslennikov, Ph.D., Chair

Simin Rahighi, Ph.D.

Rennolds Ostrom, Ph.D.

The thesis of Wonsuk Choi is approved.

DocuSigned by:
Innokentiy Maslennikov
40E3B8E7880C4A...

Innokentiy Maslennikov, Ph.D., Chair

DocuSigned by:
Simin Rahighi
71E1842ACB294C2...

Simin Rahighi, Ph.D.

DocuSigned by:
Rennolds Ostrom
776728D5D56949D...

Rennolds Ostrom, Ph.D.

August 2023

Analyzing Functional Interactions of Designed Peptides by

NMR Spectroscopy

Copyright © 2023

by Wonsuk Choi

ACKNOWLEDGEMENTS

I am thankful for the love and support from my family and friends in Chicago, Illinois; Iowa City, Iowa; Irvine, California; and Korea. Their advice and company helped me through the program and motivated me to write this paper.

I want to make a special mention of a moment I shared with my grandfather(최영렬). While visiting him, we went out for an errand and stopped at a local park gazebo in Chang Won, Korea. My grandfather, who rarely spoke, talked about his experiences at my age. He then calmly looked into the sky and told me he hoped I would live my life to the fullest; the program and this paper are the results of his advice.

I would also like to thank my committee members for their support and patience. With their flexibility and guidance, I gained the scientific experiences and exposure I had in this program.

ABSTRACT

Analyzing Functional Interactions of Designed Peptides by NMR Spectroscopy

by Wonsuk Choi

The development of small peptide-based therapeutics can be accelerated by the knowledge of relationships between the peptide structure and its functional interactions. Here, we report the analysis of two groups of synthetic peptides designed for two applications – broad bactericidal action and inhibition of protein-protein interactions in human cells. Novel amphiphilic peptides designed for antibacterial application incorporated arginine as cationic amino acids and non-natural amino acids that have aromatic side chains with similar hydrophobic properties as tryptophan. The interaction of lead cyclic peptides and their linear analogs with a phospholipid bilayer mimicking a bacterial membrane was studied using nuclear magnetic resonance (NMR) spectroscopy. These results provided insight into the mechanism of peptide bactericidal action and the role of the peptide structure in their activity. In the second example, we perform a structural characterization of a peptide designed to modulate the activation of the NF-kappaB signaling pathway. The peptide was designed to mimic the spatial structure of the HOIP-NZF1 domain interacting with the NEMO CC2-LZ domain to suppress the NF-kappaB activation. The structure elucidation of the designed peptide provided vital information about matching the required pharmacophore structure in the peptide.

TABLE OF CONTENTS

	<u>Page</u>
ACKNOWLEDGEMENTS	IV
ABSTRACT	V
LIST OF TABLES	VII
LIST OF FIGURES	VIII
LIST OF ABBREVIATIONS	X
1. INTRODUCTION	1
1.1. Peptide Therapeutics	1
1.2. Natural and Synthetic Antimicrobial Peptides	3
1.3. NF-kappaB and Peptides as Blockers of Protein-Protein Interaction	5
1.4. Linear Ubiquitin Chain Assembly Complex.....	5
1.5. HOIP Interactions with NEMO	6
1.6. Structure-Based Drug Design	7
1.7. NMR Spectroscopy Studies the Structure and Interactions of Potential Drugs and Lead Compounds	9
1.8. Physical Background of NMR Spectroscopy	9
1.9. 1D and 2D NMR Experiments.....	14
1.10. NMR Structure Determination.....	16
2. METHODS	17
2.1. Peptide Synthesis and Purification.....	17
2.2. NMR Experiments	18
2.3. NMR Signal Assignment	19
2.4. NMR Data Analysis.....	20
3. RESULTS	22
3.1. Analysis of Potent Antimicrobial Peptides	22
3.1.1. Assignment of NMR spectra.....	25
3.1.2. Peptide-Membrane Interactions	30
3.1.3. SAR of Cyclic and Linear Peptides	33
3.2. Spatial Structure of the Peptide HP2	35
3.2.1. Preliminary NMR Analysis.....	35
3.2.2. NMR Assignment	37
3.2.3. Structure Calculation and Analysis.....	41
3.2.4. Conformational Heterogeneity of HP2	43
3.2.5. Structure of HP2 in Comparison with HOIP NZF1	49
4. CONCLUSION	53
5. REFERENCES	56

LIST OF TABLES

	<u>Page</u>
Table 1. Chemical shifts of peptides 8L and 9L in water at 25 °C	29
Table 2. Amino acid sequences of the peptide HP2 and the corresponding region of HOIP	35
Table 3. Chemical shift table of HP2-2	41
Table 4. Statistic for the best 20 structures calculated for the Primary conformation	43
Table 5. Statistic for the best 20 structures calculated for the Secondary conformation	43
Table 6. Types of interaction between HOIP and NEMO	53

LIST OF FIGURES

	<u>Page</u>
Figure 1. Ribbon representation of the X-ray structure (PDB ID: 4OWF) of NEMO fragment in complex with HOIP NZF1 domain.	6
Figure 2. X-ray structure (PDB ID: 4OWF) of NEMO-binding region of HOIP-NZF1 (residues 365-379). Blue dotted lines represent hydrogen bonds that stabilize the spatial structure of the NZF1 domain.	7
Figure 3. Flow Chart of structural determination within the structure-based drug.	8
Figure 4. Cross-peak integration using a model-based linear fitting approach.	21
Figure 5. Chemical structures of unnatural amino acids: 3,3-diphenyl-L-alanine (Dip, Left panel) and 3-(2-naphthyl)-L-alanine (Nal, Right panel).	23
Figure 6. TOCSY spectra (H^N region) of peptide 8L in water..	24
Figure 7. NOESY spectrum of peptide 8L.	25
Figure 8. Strip representation of NOESY spectrum of peptide 8L.	26
Figure 9. TOCSY spectra (H^N region) of peptide 9L in water..	27
Figure 10. Strip representation of NOESY spectrum of peptide 9L.	28
Figure 11. Interaction of peptide 8L with DOPC/DOPG (75/25) liposomes monitored by 1H-NMR at four lipid:peptide molar ratios.	30
Figure 12. Interaction of peptide 9L with DOPC/DOPG (75/25) liposomes monitored by 1H-NMR at four lipid:peptide molar ratios..	31
Figure 13. Long-range inter-residue contacts were detected in the NOESY spectrum of peptide 8L in the presence of the liposomes.	32
Figure 14. Overlay of TOCSY spectra of two fractions of peptide HP2	36
Figure 15. TOCSY spectrum of HP2.	37
Figure 16. TOCSY close-up of duplicated Glu 11 (left) and Arg 12 (right) spin systems.	38
Figure 17. H^N region of the NOESY spectrum of HP2.	39

Figure 18. Strip representation of NOESY spectrum of HP2.	40
Figure 19. Superposition of the best structures from the primary (blue) and secondary (orange) conformations sets..	44
Figure 20. Best HP2 structures of primary (blue) and secondary (orange) conformation.	45
Figure 21. 20 Best HP2 structures of primary conformation.	46
Figure 22. 20 Best HP2 structures of secondary conformation.	47
Figure 23. The sequence distribution of the number of distance constraints used to calculate the primary (top bars) and secondary (bottom bars) conformations.	48
Figure 24. NEMO and HOIP ³⁶⁵⁻³⁷⁹ interacting side chains pairs – electrostatic (Yellow), hydrophobic (Red), hydrogen bond (White)	49
Figure 25. Frontal view of the NEMO-HOIP interacting side chains hydrophobic (Red) and electrostatic (Yellow)	50
Figure 26. NZF1 domain of HOIP orientation on NEMO hydrophobicity surface..	51
Figure 27. Interactions within HOIP ³⁶⁵⁻³⁷⁹ that stabilize the conformation of NZF1 domain...	51
Figure 28. Primary and secondary conformation of peptide HP2 aligned to HOIP structure next to NEMO	52

LIST OF ABBREVIATIONS

<u>Abbreviation</u>	<u>Meaning</u>
AMP	Anti-Microbial Peptide
COSY	Correlation Spectroscopy
DIP	3,3-Diphenyl-L-alanine
DOPC	Dioleoylphosphatidylcholine
DOPG	Dioleoylphosphatidylglycerol
FID	Free-Induction Decay Signal
FT	Fourier Transformation
HMBC	Heteronuclear Multiple Bond Correlation
HOIP	HOIL-1-Interacting Protein
HPLC	High-Performance Liquid Chromatography
HSQC	Heteronuclear Single Quantum Coherence
HTS	High-Throughput Screening
IKK	I κ B kinase complex
LUBAC	Linear Ubiquitin Chain Assembly Complex Ligase
MALDI MS	Matrix-Assisted Laser Desorption/Ionization-Mass Spectroscopy
Nal	3-(2-naphthyl)-L-alanine
NEMO	Nuclear Factor-kappa Beta Essential Modulator
NF-kB	Nuclear factor-kappa beta
NMR	Nuclear Magnetic Resonance
NOE	Nuclear Overhauser Effect
NOESY	Nuclear Overhauser Enhancement Spectroscopy

NZF	NPL4 Zinc-Finger
NZF1	HOIP Zinc-Finger Region 1
PC	Phosphatidylcholine
PDB	Protein Data Bank
PG	Phosphatidylglycerol
PPI	Protein-Protein Interaction
RF	Radiofrequency
TOCSY	Total Correlation Spectroscopy

1. Introduction

The study aimed at the structure and functional interactions of the peptides designed for therapeutic applications. The project consists of two aims using NMR spectroscopy methods for structural and molecular interaction analysis.

Aim 1 focuses on NMR spectroscopy analysis of lead amphiphilic peptides that show promising broad-spectrum antibacterial activity and fast bactericidal action. We studied the role of peptides' chemical and spatial structure on their interactions with liposomes that mimic the bacterial membrane. The study provided valuable insight into the design of novel drugs potent against antibiotic-resistant bacteria.

In Aim 2, we studied the spatial structure of the peptide designed based on the amino acid sequence of NZF-1 region (residues 365-379) of LUBAC subunit HOIP. We studied the spatial structure of this peptide in solution using 2D NMR spectroscopy to see how the synthetic peptide mimics its natural prototype's structure and pharmacophore characteristics. This project provides valuable information for future strategies of peptide design aiming to represent the structure of the active site of a large protein.

1.1. Peptide Therapeutics

All aspects of biological functions, such as cell growth, differentiation, and death, are influenced by protein-protein interactions (PPIs). Thus, attempts to modulate these functions lead to developing novel therapeutic candidates that should affect the PPIs (Andrews et al., 2004). Peptides are considered perfect candidates as they closely mimic the protein's principal features. They can be quickly produced and modified to improve their stability, binding strength, and bioavailability, among other properties (Giralt et al., 2015). Given that many obvious peptide targets have been resolved, it is necessary to explore new routes of peptide design. Some new

areas of interest include multifunctional cell-penetrating peptides and drug conjugates (Fosgerau et al., 2014). Therapeutic applications of peptides extend from traditional use as biomarkers and antimicrobial drugs to treating cancers, metabolic, and inflammatory diseases. Peptides are becoming recognized as a valid, potent, and safe method to target previously ‘undruggable’ targets. In the last two decades, more than 60 peptide medicines have been approved by the FDA, more than 100 are in clinical trials, and several hundred are in pre-clinical trials (Deber et al., 2017).

New compounds that are synthesized in medicinal chemistry labs are considered ‘drug-like’ if they comply with the criteria of Lipinski’s Rule of 5 (Lipinski et al., 2001). The rules describe molecular characteristics such as molecular weight (<500Da), the number of H-bond donors (equal or less than 5), acceptors (similar or less than 10), and log P (less than 5). If a drug fulfills these requirements, it is considered orally bioavailable, the most convenient and preferred method of drug delivery, as the patients can independently administer the dose (Cooper et al., 2020). However, most of the peptides are relatively large (>500 Da) and do not meet the molecular weight criteria of the Rule of 5. Also, they are susceptible to acidic and enzymatic degradation within the gastrointestinal tract and have difficulty crossing intestinal mucosa by active or passive diffusion (Pollastri et al., 2010). To address the challenges in converting a peptide that is active *in vitro* into a prospective compound with significant activity *in vivo*, we need to understand its structure-function relationships and interactions with targets at the atomic level. The ability to control its 3D shape enables the design of the molecules, opening the potential to target and modulate cellular signaling processes constraining the peptides to specific active conformation can be used to aid in yielding high-affinity compounds to be structurally stable and resistant to degradation by proteases (Kaspar et al., 2013).

1.2. Natural and Synthetic Antimicrobial Peptides

The discovery of penicillin and antibiotics by Sir Alexander Fleming has impacted the field of medicine by saving millions of lives (Tan et al., 2015). However, in an interview, he had warned that the inappropriate use of penicillin could lead to an evolution of a resistant “mutant” form of *Staphylococcus aureus*, which could cause more serious infection in the host or those who were in contact with the host passing the resistant microbe (Alanis, 2005). Strains that have consistently been exposed to all types of antimicrobial agents for decades have developed resistance to classic antibiotics and newer agents (McGowan et al., 1996). Our failure to kill “superbugs” with the most potent antibiotics emphasizes the urgent need to develop other control agents (Bahar et al., 2013).

Natural antimicrobial peptides (AMPs) function as antibiotics and effector molecules of the innate immune system in all living systems (Maroti et al., 2011). The AMPs, synthesized in ribosomes, have been isolated from species of all kingdoms and classified by their structure and amino acid composition. Many AMPs demonstrate antimicrobial activity against a broad spectrum of pathogenic bacteria with the ability to lyse bacterial cells by interacting with the cell membranes (Koczulla et al., 2012). These peptides are positively charged and amphiphilic, i.e., they contain both hydrophobic and hydrophilic surfaces that allow interaction with different environments - aqueous, membrane surface, and hydrophobic core of the membranes (Izadpanah et al., 2005). AMPs contain 10-50 amino acid residues with an overall positive charge ranging from +2 to +9 (Hancock et al., 2006). According to the current common view, the generalized mechanism of action of AMPs is to compromise the microbial cytoplasmic membrane's stability, increase the membrane's permeability, and erode the electrochemical gradient across the membrane (Oh et al., 2014). AMPs effectively pass through the thick proteoglycan layer of

gram-positive bacteria and the lipopolysaccharide outer membrane of gram-negative bacteria (LiJianguo et al., 2017). Previous studies, including studies conducted in Dr. Parang's lab, have shown that amphiphilic antimicrobial peptides composed of four arginine (R) and four tryptophan (W) residues have exhibited activity against drug-resistant pathogens, especially *Staphylococcus aureus* (MRSA) (Oh et al., 2014). Phenylalanine, a native hydrophobic amino acid with an aromatic side chain, was also a candidate. However, it was ineffective in providing sufficient hydrophobic bulk to interact with the membrane compared to tryptophan (Riahifar et al., 2018). Arginine plays a significant role in membrane protein activity, is utilized for sensing membrane voltages, and is responsible for antimicrobial actions for toxins and cell-penetrating peptides (Li et al., 2013). The ability to interact with the membrane depended on the number of arginine residues, thus determined by the hydrophobicity-hydrophilicity (or amphiphilic) balance of the peptide surface. Modifying the amphiphilic balance altered the efficiency of peptide internalization and the internalization mechanism. Dr. Parang's lab continues to develop small therapeutics AMPs by adjusting the balance between the charge and the hydrophobic bulk to make the peptides active but not very toxic. The group created a series of peptides with non-natural aromatic amino acids (Dip/Nal) that have hydrophobic properties compared to tryptophan to study the effect of size, shape, and flexibility of hydrophobic side chains on the peptide interaction with the bacterial membrane (Lohan et al., 2022).

The bacterial cell membrane contains up to 30% of negatively charged phospholipids. In contrast, the mammalian cell membrane mostly contains zwitterionic lipids (phosphatidylcholine, PC, which has both positive and negative charges and a net zero charge) and is quite rich in cholesterol. Thus, the model liposomes are prepared from PC and phosphatidylglycerol (PG, negatively charged) to represent the bacterial membrane composition

or from PC and cholesterol to mimic the mammalian cell membrane (Mitchell et al., 2016; Dreier et al., 2019).

1.3. NF-kappaB and Peptides as Blockers of Protein-Protein Interaction

Transcription factor nuclear factor-kappa beta (NF- κ B) is a critical regulator of immune and inflammatory responses. The NF- κ B/Rel mammalian family comprises five members: p50, p52, p65, Rel-A, c-Rel, and Rel-B proteins which form homo- or heterodimers (Sivagami et al., 2018). While most combinations can exist, the typical form that activates the NF- κ B in response to extracellular signals is the heterodimer of p50 and p65 (Roff et al., 1996). For the NF- κ B to work as a transcription promoter, the p50-p65 complex needs to be translocated to the nucleus. However, in its inactive state, the complex usually rests in the cytoplasm with its inhibitor I κ B- α attached to the p65 component, restricting NF- κ B translocation into the nucleus (Brown et al., 1993). NF- κ B is only released when the I κ B- α undergoes phosphorylation, followed by ubiquitination (Roff et al., 1996). The phosphorylation that flags I κ B- α for ubiquitination is mediated by the I κ B kinase (IKK) complex composed of IKK α , IKK β , and IKK γ /nuclear factor-kappa beta essential modulator (NEMO) (Li et al., 2001). The kinase comprises IKK α and IKK β , while IKK γ /NEMO is a regulatory subunit that regulates the release of I κ B- α and NF- κ B activation (Israel, 2010).

1.4. Linear Ubiquitin Chain Assembly Complex

Linear ubiquitin chain assembly complex (LUBAC) mediates a linear polyubiquitination of NEMO that is necessary for the assembly of IKK, phosphorylation of I κ B- α , and activation of NF- κ B. It was demonstrated that the binding of linear ubiquitin chain to NEMO is significant for the activation of NF- κ B as mouse model deficient of specific LUBAC substrate impaired activation of NF- κ B (Rahighi et al., 2009; Tokunaga et al., 2011). LUBAC is composed of

HOIL-1L, HOIP, and SHARPIN subunits. The NPL4 zinc-finger (NZF) domain of the HOIP subunit is crucial in recruiting NEMO and subsequent conjugation of linear ubiquitin chains to NEMO (Niu et al., 2011). Each subunit of LUBAC has been expressed with or without NEMO, and HOIP co-immunoprecipitated with NEMO (Hiroaki et al., 2014).

1.5. HOIP Interactions with NEMO

Studies of the interactions between LUBAC and NEMO show that HOIP is the primary substrate, the only LUBAC subunit that co-immunoprecipitated with NEMO. Within HOIP, zinc finger regions were individually deleted to observe their effect on the binding to

NEMO. Compared to other zinc-finger regions, the deletion of the HOIP Zinc-finger region 1 (NZF1) most substantially reduced HOIP binding to NEMO. Conversely, HOIP mutants containing only one zinc finger region, NZF1, could bind to NEMO but not ZF or NZF2. These results strongly suggest the responsibility of HOIP-NZF1 in recruiting NEMO (Hiroaki et al.,

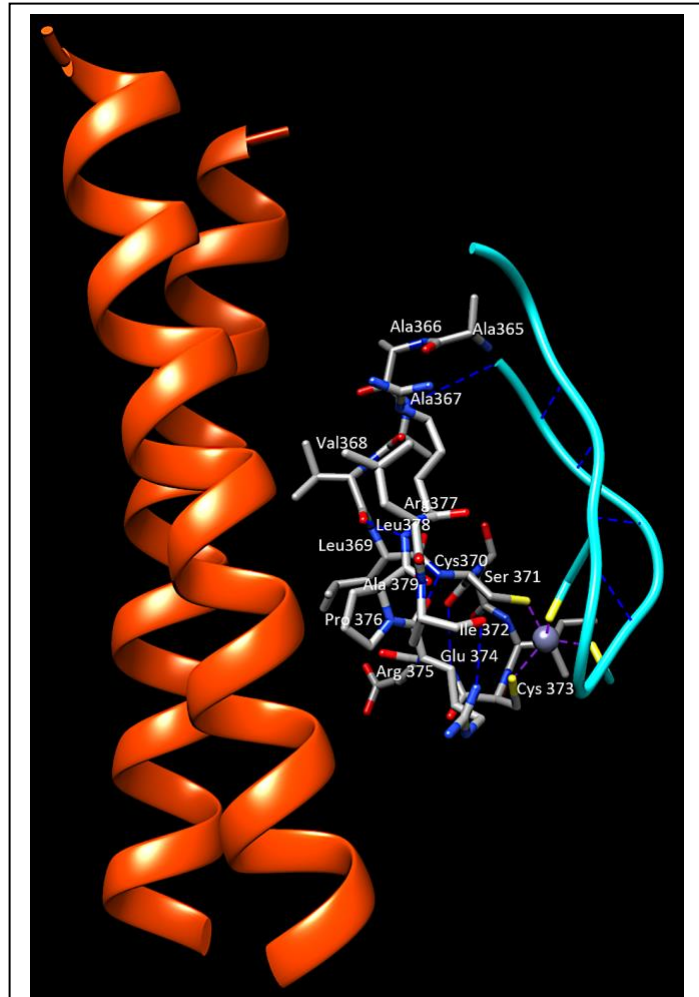


Figure 1. Ribbon representation of the X-ray structure (PDB ID: 4OWF) of NEMO fragment (residues 252-276 shown, left two orange ribbons) in complex with HOIP NZF1 domain fragment (cyan ribbon for residues 351-364, grey stick representation for residues 365-379). The zinc atom (gray) is shown coordinated by four cysteine side chains (yellow) of NZF1.

2014). The spatial structure of the HOIP NZF1-NEMO complex (PDB: 4OWF, Figure 1) shows close interaction of NZF1 fragment 351-379 with a helical dimer of NEMO. The strength of such surface-surface interaction is usually determined by the complementarity of the surfaces on both proteins, which, in turn, is defined by the localization of different types of side chains (charged, hydrophilic, and hydrophobic) on the structured surface and formation of multiple point-to-point electrostatic and hydrogen bonded contacts, as well as geometrical alignment and fit of the extended hydrophobic area formed by certain side chains. The spatial structure of the NEMO helical dimer is well-defined and constrained. Similarly, the compact fold of the HOIP NZF1 domain is constrained by four Cysteine residues coordinating the Zn²⁺ ion and several hydrogen bonds that stabilize the backbone structure of the HOIP NZF1 region (Figure 2).

1.6. Structure-Based Drug Design

Structure-based drug design utilizes the knowledge of the three-dimensional structures of a drug and/or a target molecule to guide drug discovery (Colman, 1994). The development of these methods allows the transition from the traditional drug discovery process, where lead identification is achieved

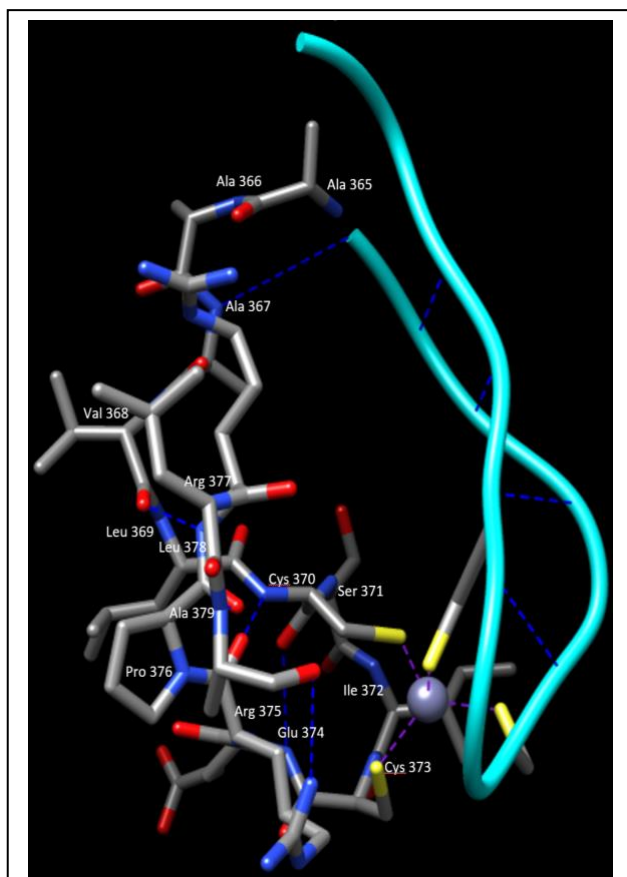
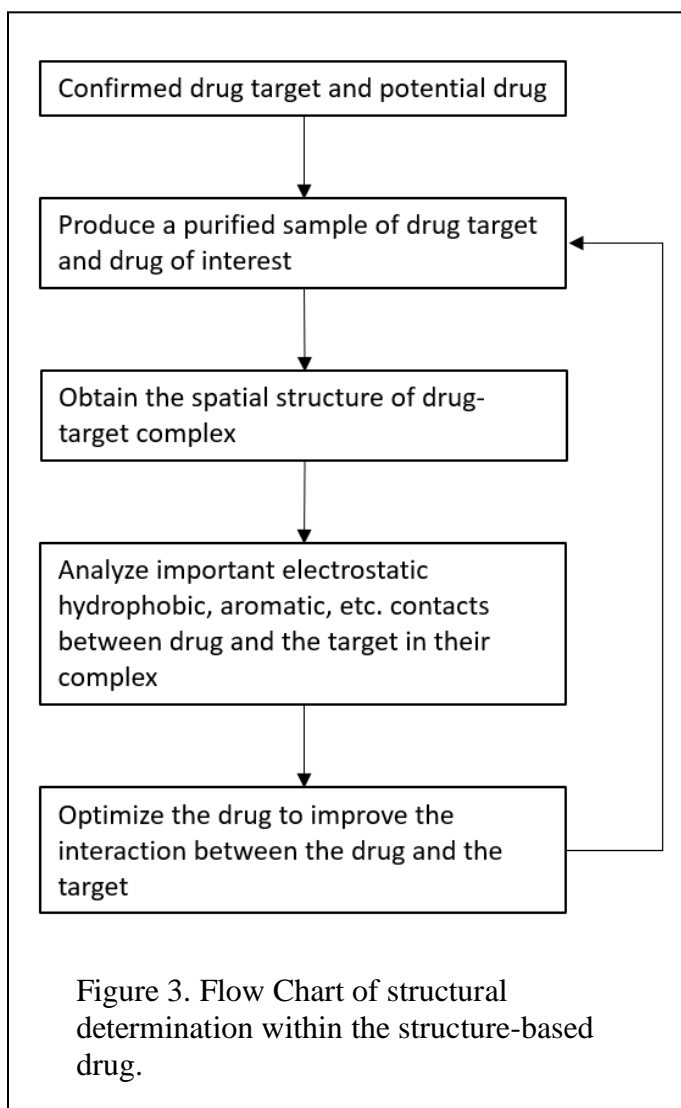


Figure 2. X-ray structure (PDB ID: 4OWF) of NEMO-binding region of HOIP-NZF1 (residues 365-379). The C-C bonds are shown in gray, Oxygen in red, Nitrogen in blue, and Sulfur in yellow. The Zinc atom is shown as a grey sphere. Blue dotted lines represent hydrogen bonds that stabilize the spatial structure of the NZF1 domain.

by experimental high-throughput screening (HTS), to rational, structure-based drug discovery and design (Amzel, 1998; Cheng et al., 2012). The transition to rational drug design and the discovery of novel therapies can be credited to several technological and scientific advancements in the last few decades. Among them are powerful and user-friendly computers, development of comprehensive statistical tools that utilize theoretical or experimental data and allow quantitative analysis of structure-activity relationships, new methodologies in theoretical calculations of the total energy of the drug-target system for optimizing the drug geometry, and the development of powerful experimental techniques, such as X-ray crystallography and NMR spectroscopy, for atomic-level structural characterization of drugs, drug targets, as well as studies of drug-target interactions

(Mavromoustakos et al., 2011). These advancements provide rational drug design with efficiency, cost-effectiveness, and time-saving to help predict and overcome possible toxic side effects at the design stage (Mandal et al., 2009).

The iterative process of structure-based drug design (Figure 3) consists of producing a purified sample of the target molecule, natural ligand, and/or drug suitable for the structural studies; analysis of their spatial structure by either X-ray



crystallography or NMR spectroscopy; data processing and structure elucidation by computer algorithms; analysis of the obtained structural and interaction data and optimization of the lead molecule chemical structure to improve binding affinity and specificity to the target; repeat the process with the optimized lead molecule to confirm the expected improvement in binding and specificity (Anderson, 2003).

1.7. NMR Spectroscopy Studies the Structure and Interactions of Potential Drugs and Lead Compounds

Solution NMR spectroscopy is a powerful and unique tool for investigating molecular systems and their functional interactions for structure-based drug design applications. It is highly versatile in analyzing small to large molecules, exceptionally rich in information with atomic-level details of drug and target structure and their interaction, and less prone to artifacts because the experiment is conducted in a natural-like environment (Carneiro et al., 2010).

Multiple NMR methods are used in drug design. Detection of through-bond correlations by homo- (TOCSY) and heteronuclear (HSQC, HMBC) experiments is instrumental in establishing chemical connections that are invaluable for structural analysis. Other NMR experiments, such as NOESY, utilize through-space interactions between atoms to provide data about the spatial structure of molecules and the relative positions of the interacting molecules (Pastor et al., 2008). These data contribute to the structural determination of biomolecules and ligands, structural analysis of ligand-target complexes, and ligand screening, especially when other structural biology methods fail to yield atomic-resolution results (Carneiro et al., 2017).

1.8. Physical Background of NMR Spectroscopy

According to *NMR of Proteins and Nucleic Acids* (Wuthrich, 1986) and *Protein NMR Spectroscopy: Principles and Practice* (Cavanagh et al., 2007), Nuclear magnetic resonance

spectroscopy utilizes magnetic properties of the atomic nucleus to detect signals from individual atoms that can be used to obtain information about the chemical environment of the nuclei, including the chemical and spatial structure and interactions of the molecules. A charged particle that moves in a magnetic field behaves as a dipole and generates its magnetic field. The responsiveness of atomic nuclei as charged particles to the external magnetic field strictly depends on the spin quantum number of the atom, which reflects the composition of a nucleus, precisely the number of protons and neutrons. Nuclei with an even number of neutrons and protons (^{12}C and ^{16}O) have zero spin ($I=0$) and do not interact with the magnetic field. In turn, nuclei with an odd number of neutrons and protons (for example, ^2H and ^{14}N) having integer spin ($I=1,2,3$) and nuclei with an odd mass number (^1H , ^{13}C , ^{15}N , ^{19}F , etc.) having half-integer spin ($I=1/2,3/2,5/2$) interact with the magnetic field.

Without an external magnetic field, a vector of the magnetic moment of nuclei has a random orientation. However, upon interaction with a magnetic field, the vector of the magnetic moment of nuclei with a non-zero spin will accept two or more specific orientations relative to the direction of the external magnetic field. These orientations correspond to the optimal energy levels and are defined by the magnetic quantum number (m), which takes integer values from $-I$ to $+I$. For example, energy levels for deuterium atoms ($I=1$) represent three different orientations with $m = -1, 0, \text{ and } 1$. The energy levels for sodium (^{23}Na , $I=2/3$) would be characterized by four orientations with $m = \frac{-3}{2}, \frac{-1}{2}, \frac{1}{2}, \text{ and } \frac{3}{2}$. Positive values of m correspond to the parallel orientation of the vector with respect to the external magnetic field and lower energy states. Negative values of m correspond to the antiparallel orientation and higher energy states. The difference in the energy between these orientations (ΔE) depends on the strength of the applied external magnetic field (B_0) and the nucleus gyromagnetic ratio (γ):

$$\Delta E = \frac{\gamma \pi \hbar B_0}{2\pi} \quad (1.1),$$

Where \hbar is Planck's constant.

The difference between high and low energy states (ΔE) can be detected by an NMR spectrometer as a resonance signal specific to a nucleus. The ratio between two nuclear energy states (N_β and N_α) is described by the Boltzmann equation:

$$\frac{N_\beta}{N_\alpha} = e^{\frac{\Delta E}{kT}} \quad (1.2),$$

Where T is the absolute temperature and k is the Boltzmann constant.

The equation indicates that the two nuclear states are almost equally populated at room temperature. Therefore, despite the large number of molecules in the NMR sample, only a fraction contributes to the NMR signal. Since the difference in population of the energy levels produces the NMR signal, the NMR, as a method, has relatively low sensitivity. However, it is possible to increase the difference in energy levels (ΔE) and magnetic resonance sensitivity by increasing the strength of an external magnetic field or, for example, by taking advantage of a proton's ability to absorb additional energy from photons. Radiofrequency (RF), which results in the excitation and absorption of energy by a nucleus, is also known as a resonance frequency of the nucleus. The Planck equation can calculate the electromagnetic energy absorbed by a nucleus:

$$E = \hbar \nu_0 \quad (1.3),$$

Where \hbar is Planck's constant and ν_0 is a resonance frequency.

As the excitation of a nucleus ultimately leads to the difference between the two energy states, it is essential for the resonance that electromagnetic energy matches the difference in energy levels for the nucleus:

$$\Delta E = \frac{\gamma \pi \hbar B_o}{2\pi} = \hbar \nu_o \quad (1.4).$$

Modern spectrometers use intense, short radio frequency electromagnetic pulses to excite all the nuclei in a molecule, but spectrometers are often classified by the frequency that excites ^1H . After the excitation, every nucleus release energy absorbed at a specific radio frequency while returning to equilibrium. The time-dependence of the energy released from the nuclei of the same type is recorded in the form of a free-induction decay (FID) signal. The interpretation of this signal is problematic because it combines responses from all nuclei of the same type in a sample. So, for further understanding and analysis, the FID is converted from a time-domain to a frequency-domain spectrum using a mathematical operation called Fourier Transformation (FT). For example, with chloroform, as there is only one type of proton, the energy is absorbed and released at only one RF, leading to frequency domain ^1H -spectrum containing a single proton signal.

Nuclei consist of protons and neutrons but are within a cloud of electrons. In an external magnetic field, moving electrons produce a local magnetic field (B_i) that opposes the applied external magnetic field (B_o), resulting in a true magnetic field (B) that is less than the applied external field B_o : $B = B_o - B_i$.

The atom's chemical environment determines the electron density that produces the local magnetic field. For example, a nucleus affected by either a shielding effect by electron-donating groups or a de-shielding effect by electron-withdrawing groups will change its resonance frequency. Depending on the magnitude and the direction of the shielding effect of the electrons, the chemically non-equivalent nuclei resonate at different frequencies that give rise to the signals at distinct positions in NMR spectra. The NMR spectroscopy method uses magnets that induce the external magnetic field of various strengths; therefore, the same proton will resonate at

different frequencies in the spectrometers with different magnetic field strengths. This problem is addressed by the conversion of measured resonance frequency to the chemical shifts:

$$\delta = \frac{\nu_{sample} - \nu_{reference}}{\nu_{reference}}, \quad (1.5)$$

where $\nu_{reference}$ is the resonance frequency of the reference signal.

It is also important to note that the chemical shift values are anisotropic since they depend on the relative orientation of a nucleus in the molecule with respect to the applied magnetic field. For solution NMR, the molecules' fast tumbling and Brownian motion results in averaging and isotropic presentation of chemical shifts in most samples.

Electrons in the surrounding atoms determine the position of the NMR signal for every atom in a molecule. The chemically symmetrical atoms equal in chemical structure produce NMR signals with the same position in the spectra (i.e., the same chemical shifts). Vice versa, non-symmetrical and chemically non-equivalent atoms give signals at various positions. The NMR signals have three significant features: line shape and line width related to relaxation and dynamics of the nuclei, intensity (or an integral) of a signal that, in the case of ^1H -NMR, is proportional to the number of hydrogens contributing to the signal and splitting of the signal into components (signal coupling). The different energy states of neighboring atoms (2-3 chemical bonds apart) affect the NMR signals and appear as a splitting of the signals to the several components representing different energy states of these neighboring atoms. Depending on the number of coupled atoms (n) and spin quantum number (I), the number of signal components (NS) can be calculated with a formula:

$$NS = 2nI + 1. \quad (1.6)$$

However, it should be noted that coupling between nuclei is not observable if they have equivalent chemical shifts.

1.9. 1D and 2D NMR Experiments

The information described so far has been fundamentals of NMR in one-dimensional (1D) NMR spectra. For the structural studies of biomolecules, the 1D experiments were extended to include another dimension.

Naturally, further development of the method was termed two-dimensional (2D) NMR spectra as it correlates two sets of frequencies to the signal intensities. One of the first methods of 2D NMR spectra was the correlation spectroscopy (COSY) experiment. It provides information about scalarly coupled to each other protons, considering that the two scalar-coupled hydrogens resonate at different frequencies (or have different chemical shifts). The spectrum has autocorrelation peaks (i.e., H_a/H_a and H_b/H_b), which exhibit a correlation between resonances with the same chemical shifts on two axes of the spectrum as the diagonal line from left bottom to right top. The cross-peaks outside the diagonal are observed as correlating signals resonating at different frequencies between atoms. The cross-peak intensities depend on the dihedral angle of the chemical bond between the correlated atoms; thus, the intensities are proportional to the magnitude of the coupling constants. COSY experiment and its derivatives are beneficial in analyzing molecules containing large spin systems.

The total correlation spectroscopy (TOCSY) experiment visualizes the correlation between all the protons within a given spin system where magnetization can be transferred over several successfully coupled proton pairs, unlike COSY, where only the correlations between directly coupled protons are observed. TOCSY experiment and its derivatives are beneficial in analyzing samples with multiple spin systems, such as peptides, polypeptides, and small proteins. The Nuclear Overhauser Enhancement Spectroscopy (NOESY) experiment observes the net change of signal intensity (Nuclear Overhauser Effect, NOE) from a nucleus that is resonating due to the

relaxation of perturbed nuclei that are coupled to the first nucleus by chemical bonding or by proximity in space. NOESY spectra usually contain cross-peaks from the atoms separated by less than 6 Å. Because the NOE effect is based on the relaxation, additional cross-peaks will appear in NOESY spectra if atoms form a stable pathway for magnetization transfer (spin diffusion). However, there are instances where the spectra exhibit more spin systems than expected from the structure of a molecule. In these cases, the structure will likely have different conformations that create two sets of peak systems. The intensity of the NOE signal depends on the distance between coupled nuclei and the size of the molecules. Large molecules tumble slowly and relax faster than smaller molecules, thus generating stronger NOE. There are variations of NOESY experiments for analyzing small molecules with slow relaxation. Because the NOE effect is based on spatial interactions, this technique is utilized for investigating spatial relationships in molecules, starting from the analysis of stereochemistry and up to the determination of the spatial structure of proteins. NOESY experiment can also provide relaxation parameters of particular nuclei (cross-relaxation intensity and relaxation rates) that are instrumental in the analysis of the flexibility and dynamics of a molecule (Doost et al., 2019).

The Heteronuclear single quantum coherence (HSQC) experiment detects the correlation between a heteroatom and hydrogen separated by one bond. The significant advantage of HSQC is high sensitivity since it is a proton-detected experiment, consequently less time-consuming to acquire than, for example, a 1D ^{13}C -NMR experiment with a natural abundance sample. HSQC spectrum is rich in information as it contains data on directly bound ^1H and a heteroatom (^{13}C or ^{15}N), thus simultaneously providing information about chemical shifts and chemical connectivity between ^1H and the heteroatom (Fosgerau et al., 2014). The HSQC spectrum only exhibits one

peak per paired atom, allowing easy signal assignment and reduced experimental time for nuclei with low magnetization sensitivity and natural abundances (Szantay, 2015).

1.10. NMR Structure Determination

The data obtained from the NMR can be used to characterize the structure of a protein (Cavailli, 2007). NMR analysis provides data describing the ensemble of the structures of a macromolecule in solution and measuring parameters that reflect the amplitude and timescale of macromolecular dynamics at atomic resolution (Esteban-Martin et al., 2012). Apart from determining a structure, the NMR data are instrumental in analyzing drug-target interactions using the structure of a drug-target complex or interaction mapping of a drug with the specific target protein or peptide. The place of structure determination and interaction analysis in the structure-guided drug design process is shown in Figure 3.

The structural information provided by NMR spectroscopy (see description of TOCSY and NOESY experiments in section 1.10) helps identify the macromolecule's spatial structure and characterize its conformational heterogeneity. The sequential resonance assignment aids in the identification of the secondary structure type (Wuthrich, 1986). NOESY data are used to calculate the ^1H - ^1H constraints to compile a set of distance constraints complemented with angle constraints from the coupling constants for the structure determination (Emwas et al., 2015).

In the natural environment, all biological macromolecules undergo conformational changes in various amplitudes and timescales intimately linked to the biomolecule's activity (Eisenmesser et al., 2005). Describing and understanding the structural heterogeneity of biomolecules is an essential objective in structure-activity analyses (Wen et al., 2012). Due to conformational heterogeneity, biomolecules cannot be described by one unique static structure in solution. Thus, an equilibrium of multiple conformations described as an ensemble of structures

using NMR-derived structure- and time-averaged data is currently the best representation of the structural space of a biomolecule. The relative populations of conformations that biomolecules adopt in solution and rates and timescales of conformational changes provide essential information for understanding the biomolecular interactions.

Interpretation of the spectra to confirm the presence of multiple conformation states depends on the exchange rate or time rate of the exchange process of the conformations. Conformational exchange is determined as fast, intermediate, or slow depending on whether the exchange rate is higher, close to, or less than the frequency difference between NMR parameters in distinct conformation. In the case of slow conformational interconversion, distinct chemical shifts for both states can be observed in the spectra, and the intensities of the signals are proportional to the states' populations (Kleckner et al., 2012). With the fast exchange rate, spectra have a single set of signals as rapid interconversion leads to a chemical shift averaging during the detection (Maslennikov et al., 1998). In an intermediate exchange rate, the signals in the spectra are broadened as signals from the two states have strong interference during the detection period (Kleckner et al., 2012).

2. Methods

2.1. Peptide Synthesis and Purification

The amphiphilic antimicrobial peptides 8C, 9C, 8L, and 9L (Table 1) for aim 1 were synthesized and purified by Dr. Sandeep Lohan (Dr. Parang's lab). He utilized a solid-peptide synthesis protocol to produce the peptides, and cyclic peptide candidates were processed with macrocyclization after detaching the resin to achieve its cyclic structure.

Peptide HP2 representing the HOIP region interacting with NEMO (residues 365-379 of HOIP) for aim 2 was synthesized and purified in Dr. Rahighi's Lab. During the purification, 18 peptide HP2 underwent reverse-phase purification, where two fractions of the peptide with equal mass were collected at different retention times (HP2-1 and HP2-2), thus suggesting different molecular hydrophobic properties of the peptide in these fractions.

For most of the sample processing, NMR spectroscopy follows a general theme. The peptide or drug target of interest is produced by chemical synthesis or cell culturing. The peptide is then purified using analytical chemistry techniques such as high-performance liquid chromatography. When the purified sample is obtained, the sample is mixed with DI water or preferred solvent and placed within a vial that enters the NMR spectroscopy.

2.2. NMR Experiments

The amphiphilic antimicrobial peptides 8C, 9C, 8L, and 9L (Table 1) for aim 1 were synthesized and purified by Dr. Sandeep Lohan (Dr. Parang's lab). He utilized a solid-peptide synthesis protocol to produce the peptides and processed cyclic peptide candidates with macrocyclization after detaching the resin to achieve its cyclic structure.

Peptide HP2 representing the HOIP region interacting with NEMO (residues 365-379 of HOIP) for aim 2 was synthesized and purified in Dr. Rahighi's Lab. During the purification, 18 peptide HP2 underwent reverse-phase purification, where two fractions of the peptide with equal mass were collected at different retention times (HP2-1 and HP2-2), thus suggesting different molecular hydrophobic properties of the peptide in these fractions. For most of the sample processing, NMR spectroscopy follows a general theme. The peptide or drug target of interest is produced by chemical synthesis or cell culturing. The peptide is then purified using analytical chemistry techniques such as high-performance liquid chromatography. When the

purified sample is obtained, the sample is mixed with DI water or desired solvent and placed within a vial that enters the NMR spectroscopy.

2.3. NMR Signal Assignment

The processed spectra were loaded into the CARA program for the signal assignment and analysis (Keller, 1996). NMR signal assignment was performed using the traditional sequential assignment approach (Wuthrich, 1986).

First, the individual cross-peaks in the H^N - H^α region of TOCSY spectra were identified as spin system anchors. Then, the vertical peaks aligned with the anchor cross-peaks (i.e., originating from the same H^N or another identified atom) were assigned within the same spin systems. Upon identifying the cross-peaks belonging to the same spin system, the spins were tentatively assigned to a specific hydrogen atom (or group of atoms) according to the expected chemical shifts for different amino acids (Mittermaier et al., 2009). Simultaneously, the type of amino acid was determined by the pattern of observed spins in a system and their chemical shifts. For the complete assignment, including the systems missing a signal from the H^N atom, the cross-peaks were identified through the horizontal match with the known signals in NOESY or TOCSY spectra.

After all individual spin systems were identified, the NOESY spectrum was used to link separate spin systems. Every unique NOESY cross-peak that does not exist in the TOCSY spectrum was assigned to the spins with the closest chemical shift, thus creating a spin link between the separate spin systems. With the spin links identified, connected spin systems in NOESY were aligned as the NOESY strips and traced along the peptide sequence to correlate the spin systems to corresponding amino acid residues and to determine their positions within the peptide sequence.

The obtained assignment was used in the spectra of the peptides 8C, 9C, 8L, and 9L with the liposomes to determine the effect of liposomes on chemical shifts, line widths, and intensities of the peptide signals. More than expected spin systems were identified in NMR spectra of peptide HP2, which can indicate sample heterogeneity (chemical or structural). Therefore, the NMR data were separated into sets containing continuously linked spin systems during the assignment.

2.4. NMR Data Analysis

Once the assignment of the NOESY cross-peaks for peptide HP2 was complete, the NOESY spectra were used to retrieve the data for calculating peptide spatial structure. Two methods were used to calculate signal intensity in NOESY spectra: signal shape fitting and area integration. For the signal shape fitting, a peak with the most defined shape was selected as the model peak for tuning the line-shape model, which included alignment to the Gaussian curve on both the x-axis and y-axis in the 2D spectra. Then, the linear equation system based on the obtained model was used to simulate the shape and to integrate the rest of the peaks (Figure 4).

The cross-peak assignment, chemical shifts, integral intensities, and signal amplitudes were exported as a file for structure calculation. Based on the assignment of non-unique spin systems, for the structural analysis, the NMR data were further divided into three subsets: subset 1 contained the data from the regions with only one set of signals, subset 2 contained the data for the primary (based on the intensity of signals) form in the region with duplicated systems, and subset 3 contained the data for the secondary form in the same region.

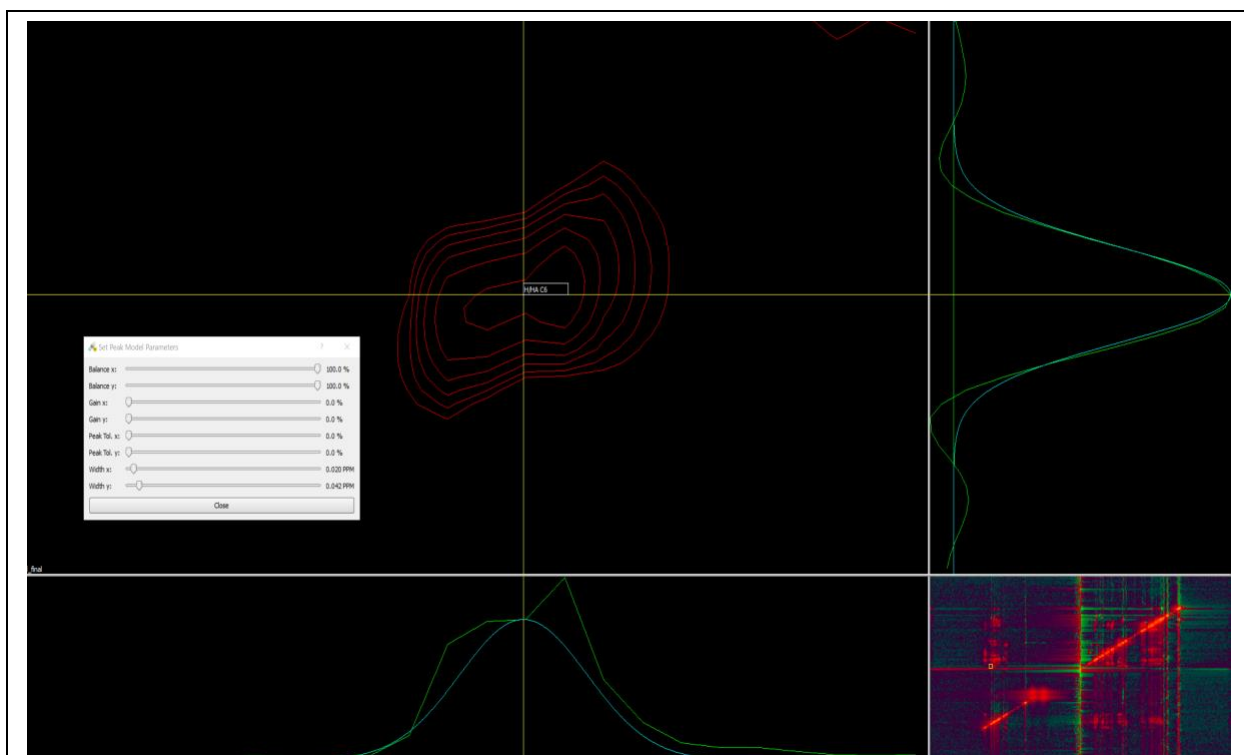


Figure 4. Cross-peak integration using a model-based linear fitting approach. A stand-alone cross-peak is utilized to calibrate the integration parameters for the spectrum. The x-axis and y-axis parameters (peak width, gain, tolerance, and balance) are modified to adjust the fitting (cyan) to match the shape of the cross-peak (green). The cross-peak shape is fitted separately – the shape on Y-axis has a good fit, but the complex shape on X-axis does not have a good fit (due to the spin-spin coupling).

CYANA program v 2.1 (www.cyana.org) was used to calculate the structure of peptide HP2. CYANA uses the known peptide sequence, proton chemical shifts, and experimental structural constraints to optimize the structure fit into the constraints (Guntert, 2008). The peptide sequence, proton chemical shifts, and the NOE constraints were exported from the CARA program after complete assignment and NOE cross-peak processing. To convert the NOE intensities into the distance constraints, the intensities were calibrated against the intensities for atom pairs with fixed distances (such as within the CH₂ groups) using the CALIBA procedure within CYANA. The three subsets of the NOE data (see above) were calibrated separately and combined in two complete sets of distance constraints for the primary and secondary forms. In

addition, the distances constraining the disulfide bond between Cys6 and Cys10 were added as recommended in CYANA.

One cycle included the calculation of 100 structures. The structural statistics, such as overall penalty function, distance constraint violations, and violations of van-der-Waals radii, were reported for the best 20 structures and analyzed. The NOESY cross-peaks corresponding to the distance constraints with strong violations (above 0.2 Å) were checked for assignment accuracy and integration or overlap with other signals in the CARA program. If necessary, the assignment or the integration were corrected. Calculating the structure and checking the distance constraints violations were repeated until all substantial violations (above 0.2 Å) were resolved. In addition, two alternatives, *cis* and *trans* configurations of the peptide bond for Pro8 residue, were used during the calculations with both datasets. The peptide bond configuration with the lowest target function and fewer violations were selected for every dataset. Once the experimental constraints were refined, the final 100 structures were calculated for each form, and the 20 best structural models were selected based on the target function. The 20 selected models were visualized and analyzed in the Chimera program (Pastor et al., 2008).

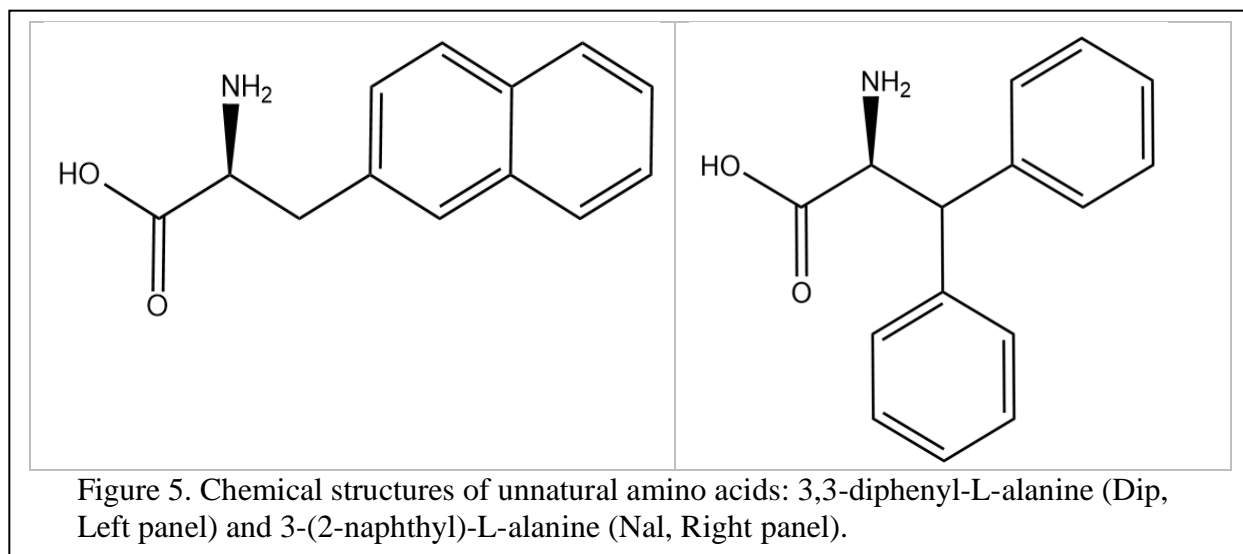
3. Results

3.1. Analysis of Potent Antimicrobial Peptides

Aim 1 is part of a large project of designing cell penetrating antimicrobial peptides that are undergoing in Dr. Keykavous Parang's lab. Two of the most active cyclic peptides and their linear analogs were selected for the NMR analysis. The selection was based on the antibacterial activity against a broad spectrum of gram-positive and gram-negative bacteria (*Enterococcus faecium*, *Staphylococcus aureus*, *Klebsiella pneumoniae*, *Acinetobacter baumannii*,

Pseudomonas aeruginosa, and *Enterobacter* species) as well as preferential cytotoxicity against bacterial over the mammalian cell (Table 1 in Lohan et al., 2022).

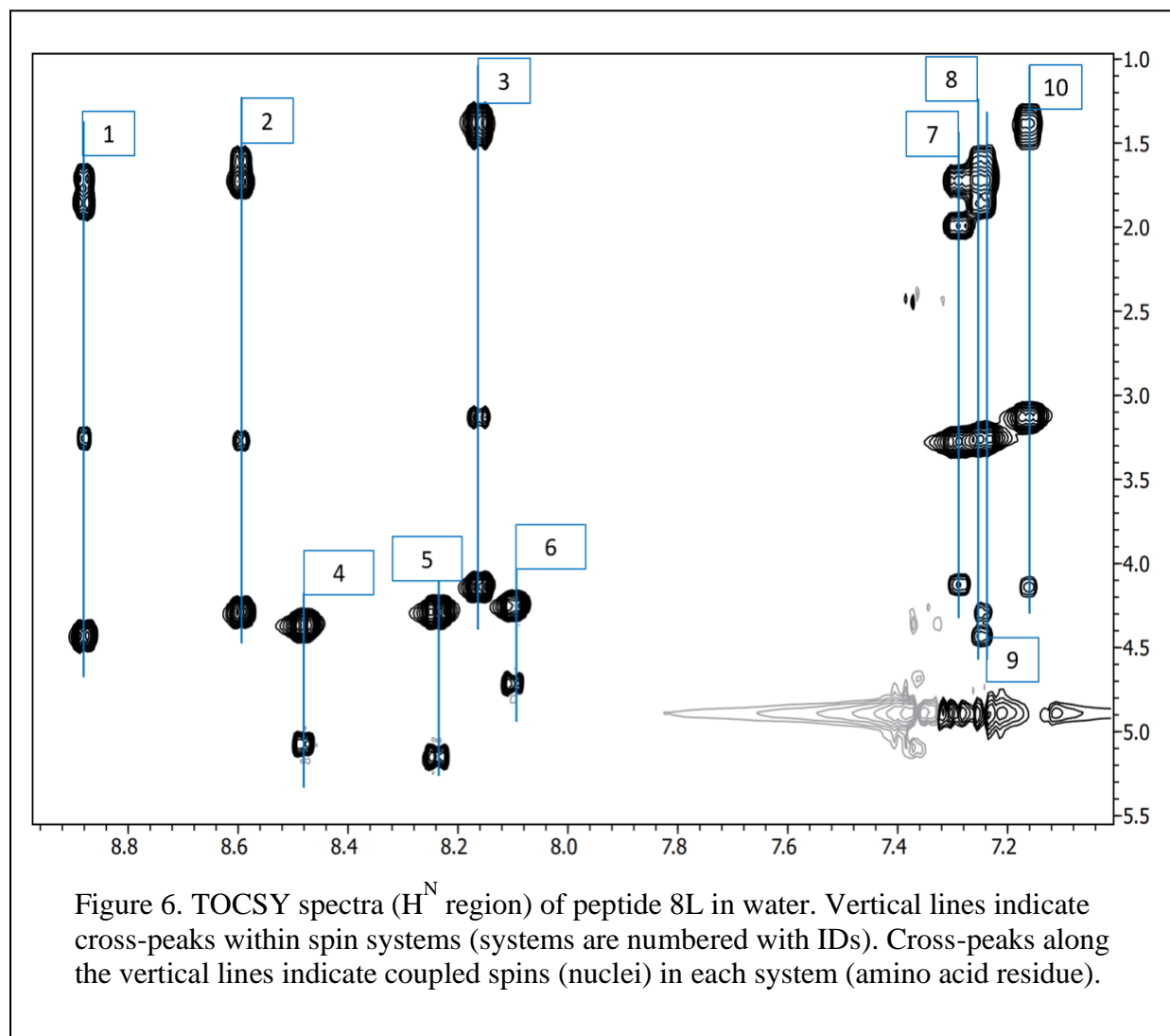
Peptides 8L, 9L (linear), 8C, and 9C (cyclic) are heptameric peptides with a sequential composition of 4 cationic residues and 3 hydrophobic unnatural residues. Peptides 8L and 8C are composed of Arginine and 3,3-Diphenyl-L-alanine (Dip); peptides 9L and 9C are composed of arginine and 3-(2-naphthyl)-L-alanine (Nal).



The chemical structures of unnatural amino acids Dip and Nal are shown in Figure 5. The cyclization of the linear peptides was conducted to improve the peptides' chemical stability and restrict the peptide backbone's flexibility, supplying more structurally rigid peptides. It is important to mention that while cyclic peptides' antibacterial activity improved overall, their hemolytic activity increased by approximately one-fold (Table 1 in Lohan et al., 2022). The peptides were synthesized, purified, tested for their activity, and prepared for NMR analysis by Dr. Sandeep Lohan.

Because of the spectral overlap and extremely fast relaxation, the resonance assignment of peptides interacting with the phospholipid bilayer can be very cumbersome. Despite their overall positive charge, cyclic peptides 8C and 9C exist primarily as high-order oligomers at

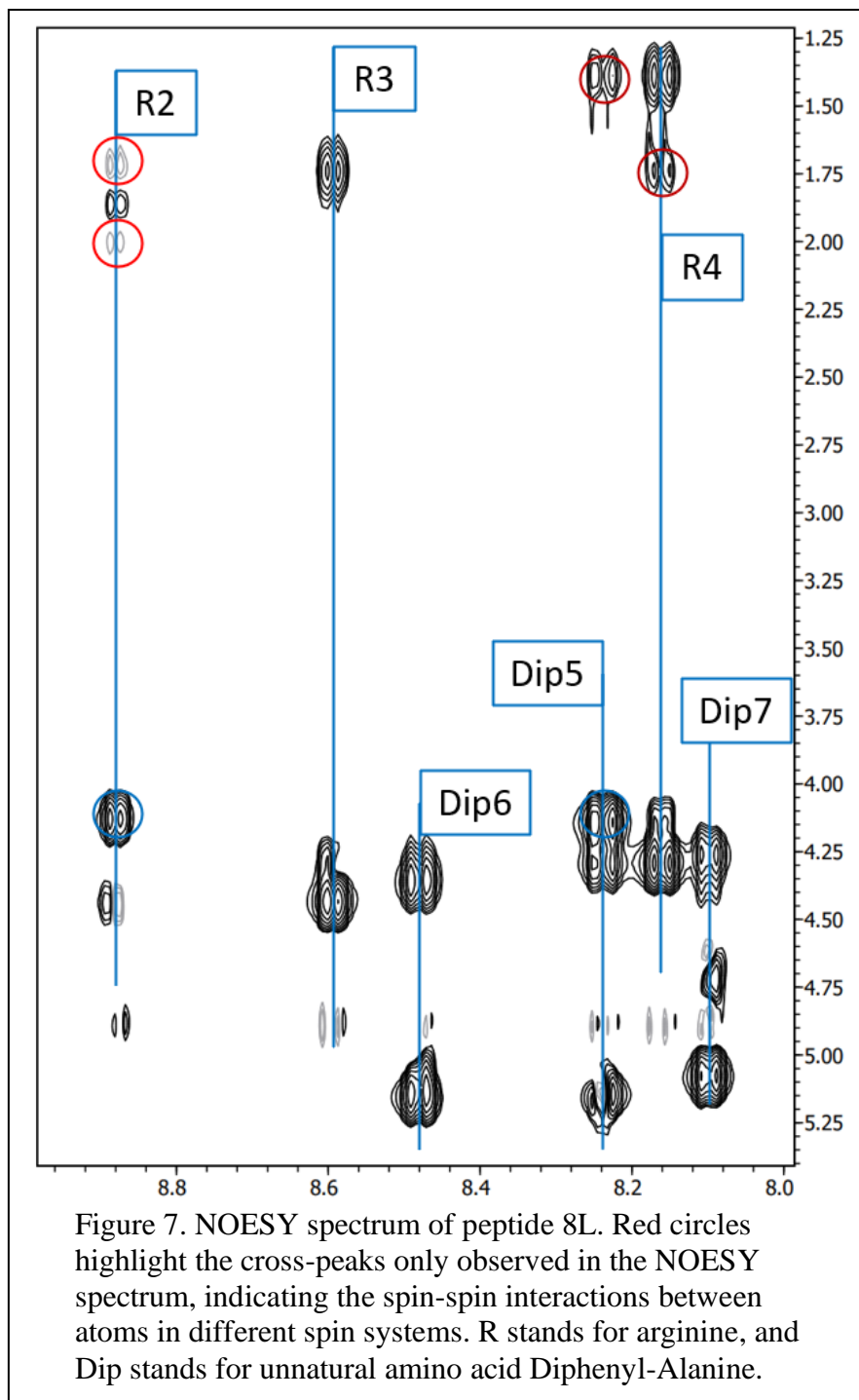
concentrations above 0.5 mM in the water, thus making the analysis of NMR spectra difficult. However, the linear peptides 8L and 9L in the same conditions show oligomerization at higher concentrations (above 1.5 mM), which provides an opportunity to reveal details of their interactions with the phospholipid bilayer by NMR spectroscopy. We first conducted a set of NMR experiments on the peptides in water to evaluate their structure. Then, we conducted the experiments gradually increasing the lipid concentration to achieve various lipid/peptide molar ratios (0:1, 1:5, 1:2, and 1:1) to analyze the peptide-lipid interactions and peptide behavior in the presence of liposomes mimicking bacterial membrane.



3.1.1. Assignment of NMR spectra

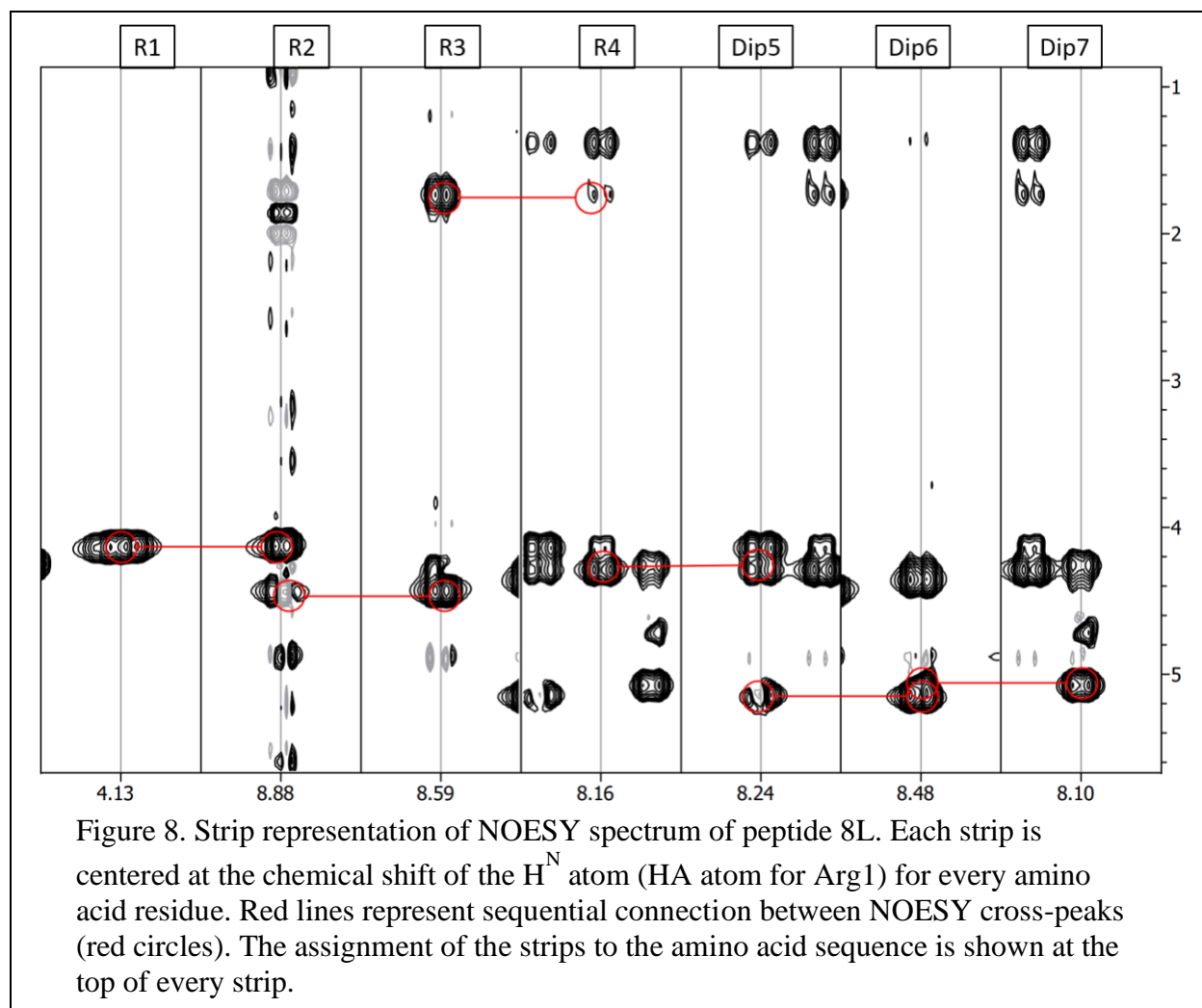
Ten distinct spin systems were determined in the TOCSY spectra of peptide 8L in water (Figure 6). The six left systems (systems 1-6 in Figure 6) originate from H^N resonances with chemical shifts of 8.0 ppm and above (x-axis); 4 additional spin systems (systems 7-10 in Figure

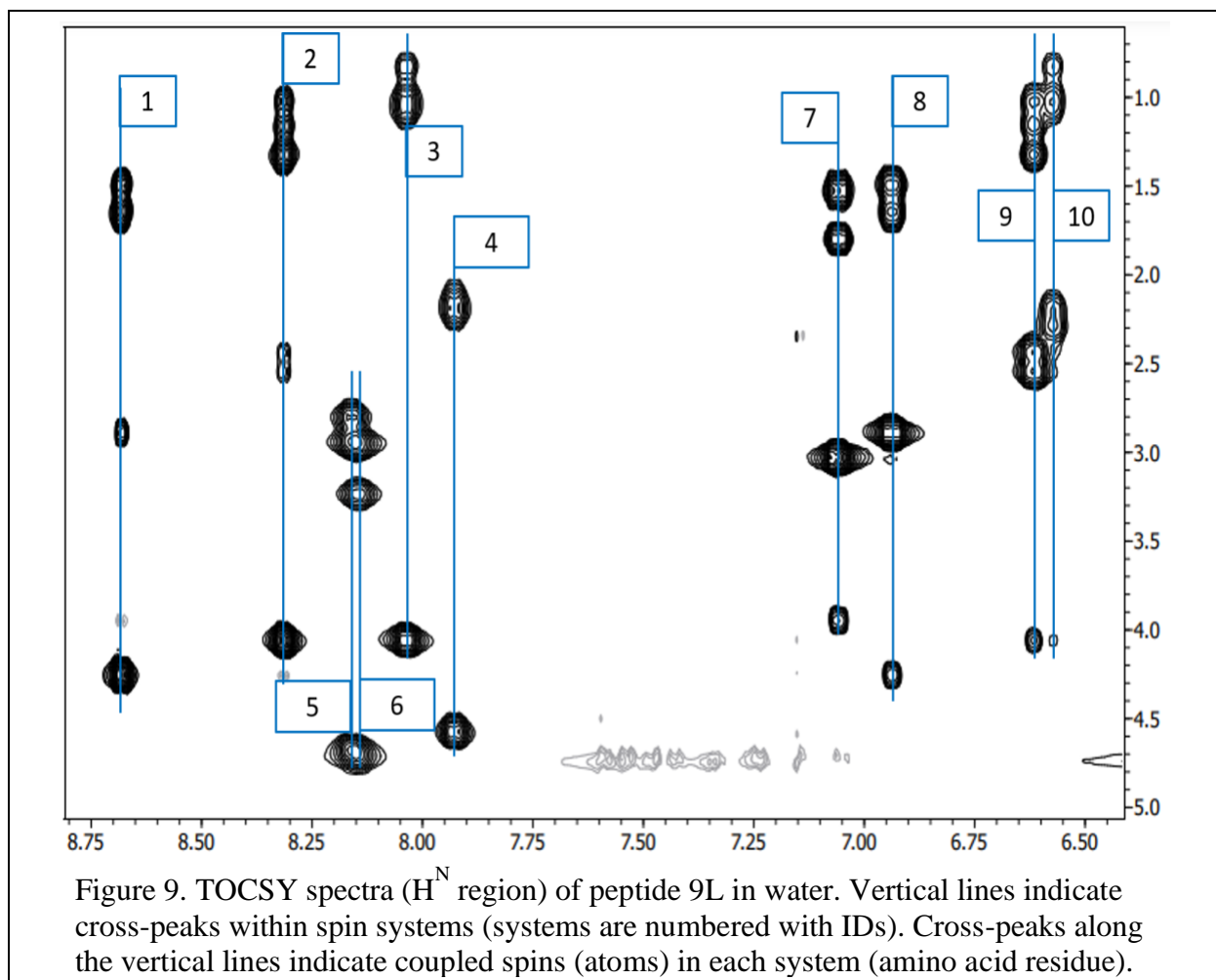
6) originate from the H^{NE} atoms in arginine sidechains with the chemical shifts below 7.6 ppm. The cross-peaks in systems 1, 2, and 3 can be linked to the corresponding cross-peaks with the same chemical shifts (vertical position) in the distinct systems 8, 9, and 10, respectively. This replication of the cross-peaks from backbone and side chain H^N atoms is characteristic of arginine spin systems and helps us to name the spin system 7



as Arg 1 (since it does not have a corresponding backbone H^N system) and systems 1/8, 2/9, and 3/10 as arginine spin systems (Figure 6). Therefore, we can assign the remaining three systems, 4, 5, and 6, to diphenylalanine residues.

Analysis of the NOESY spectrum for 8L (Figure 7) starts with identifying the cross-peaks that are not present in the TOCSY (highlighted by red circles in Figure 7). These NOESY-specific cross-peaks indicate interactions between the atoms in different spin systems, representing different amino acids in peptides and proteins. Thus, the NOESY-specific cross-peaks provide information about sequentially or spatially close spin systems, aiding in the sequential assignment of NMR spectra of a peptide or a protein.





As mentioned, the NOESY experiment provides information about atoms or atomic groups in the vicinity, including atoms in residues that are close in a peptide/protein sequence or sequentially distant atoms that are close to each other in a spatial structure. The procedure of sequential assignment of peptide 8L is demonstrated in Figure 8 with the NOESY spectrum. Strips of the NOESY spectrum showing separate spin systems are aligned to demonstrate the sequential connections between amino acid residues so we can visually follow the NOESY cross-peaks (red circles in Figure 8) to determine the order of connected spin systems in the peptide sequence. The chemical shift assignment for peptide 8L is summarized in Table 1.

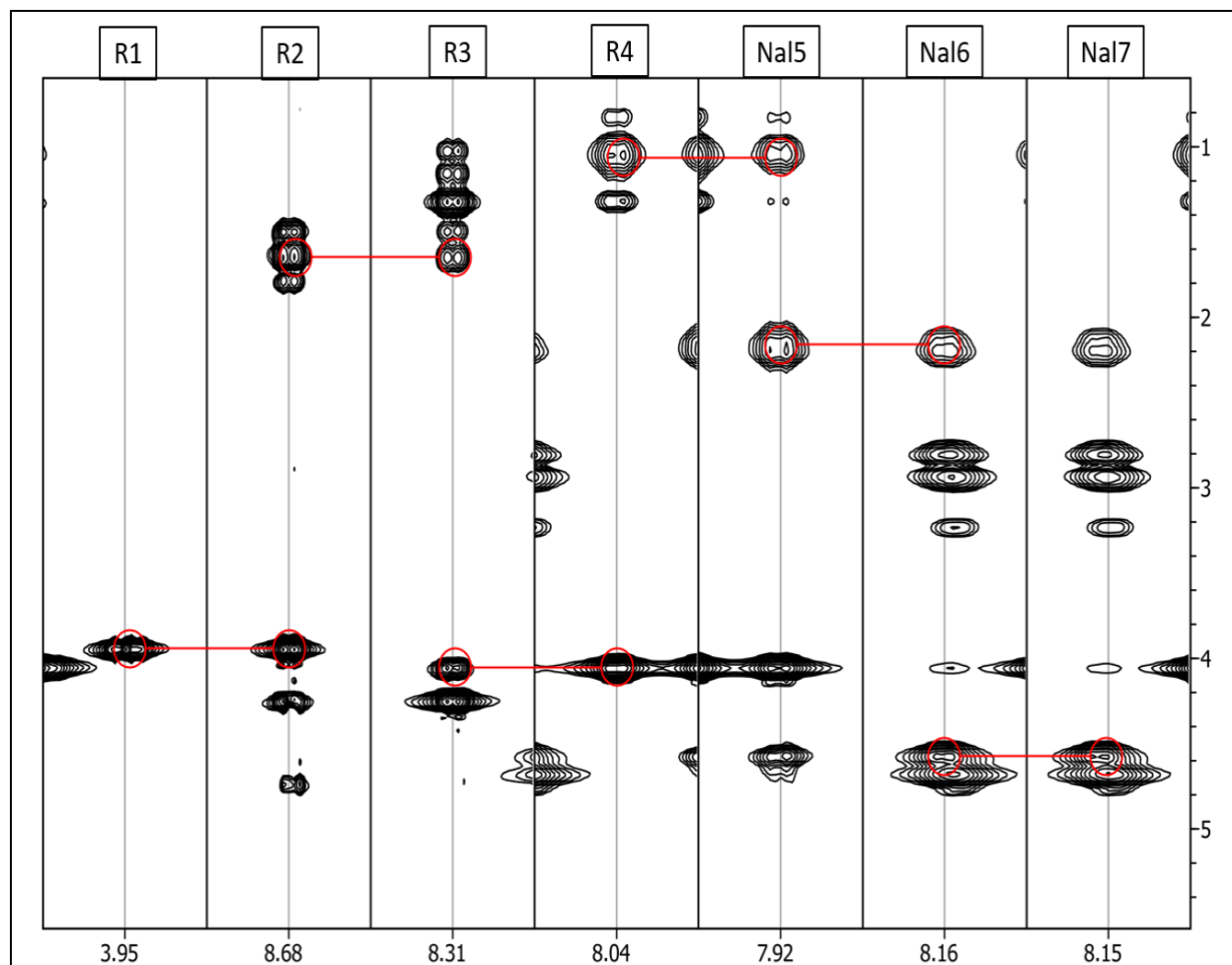


Figure 10. Strip representation of NOESY spectrum of peptide 9L. Each strip is centered at the chemical shift of the H^N atom (HA atom for Arg1) for every amino acid residue. Red lines represent sequential connectivity between NOESY cross-peaks (red circles). The assignment of the strips to the amino acid sequence is shown at the top of every strip. R stands for arginine, and Nal stands for unnatural amino acid Naphthyl-alanine.

In the TOCSY spectra for peptide 9L, four distinct systems (systems 1, 2, 3, and 4 in Figure 9) originating from H^N atoms were determined, and two systems (5 and 6) were identified upon closer inspection of overlapped cross-peaks, like 8L, systems 1, 2, and 3 show related secondary spin systems (systems 8, 9, and 10, respectively), which are the characteristics of arginine amino acids. Similar to the peptide 8L, the lack of the signal for amine for R1 is caused by the fast chemical exchange of the hydrogens in the N-terminal amino group with water. This observation indicates that system 7 in Figure 9 belongs to R1 as it does not have a paired system.

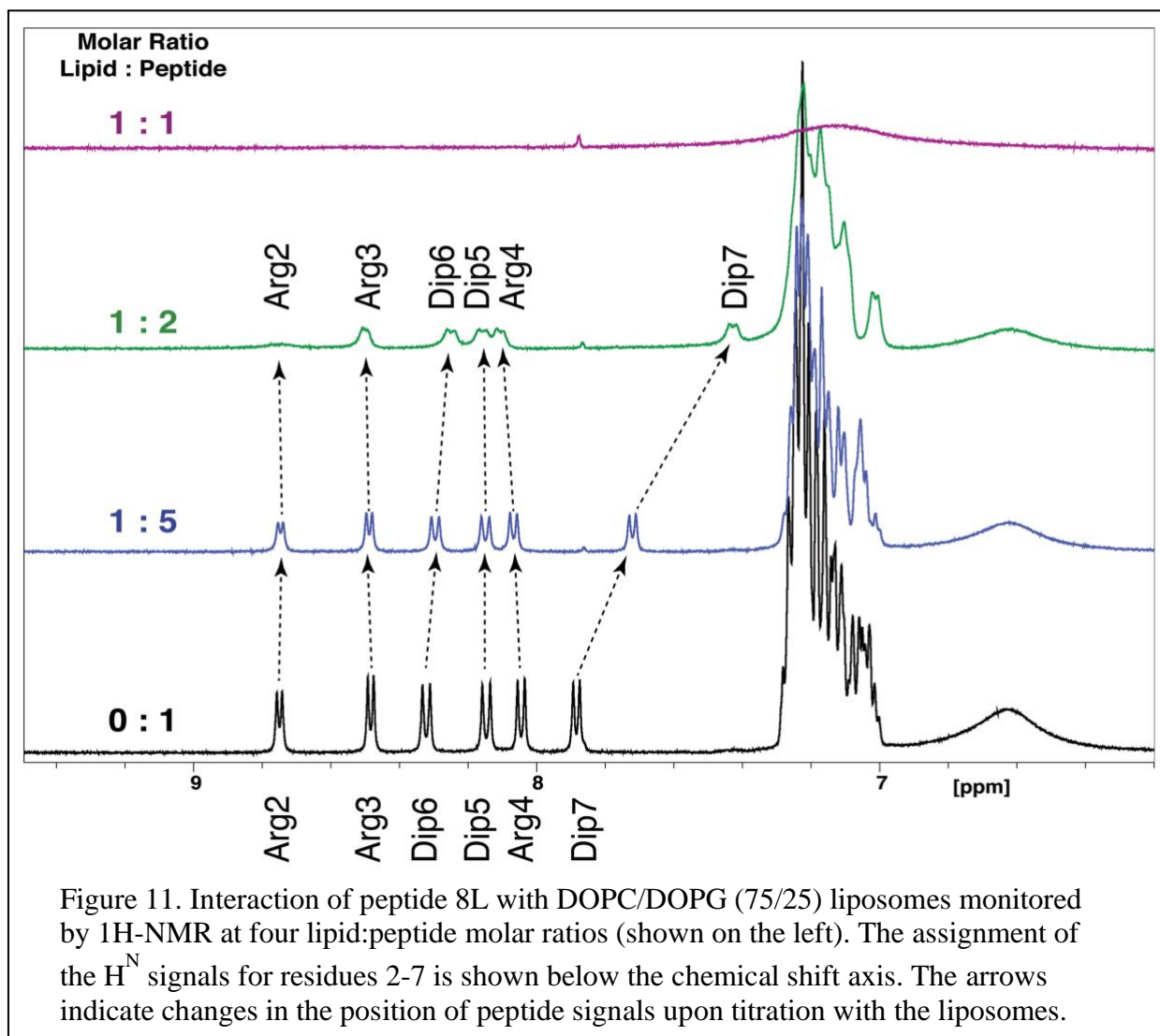
The NOESY data for peptide 9L was analyzed as described above for peptide 8L, and the sequential assignment was performed using a combination of TOCSY- and NOESY-specific data (Figures 9 and 10).

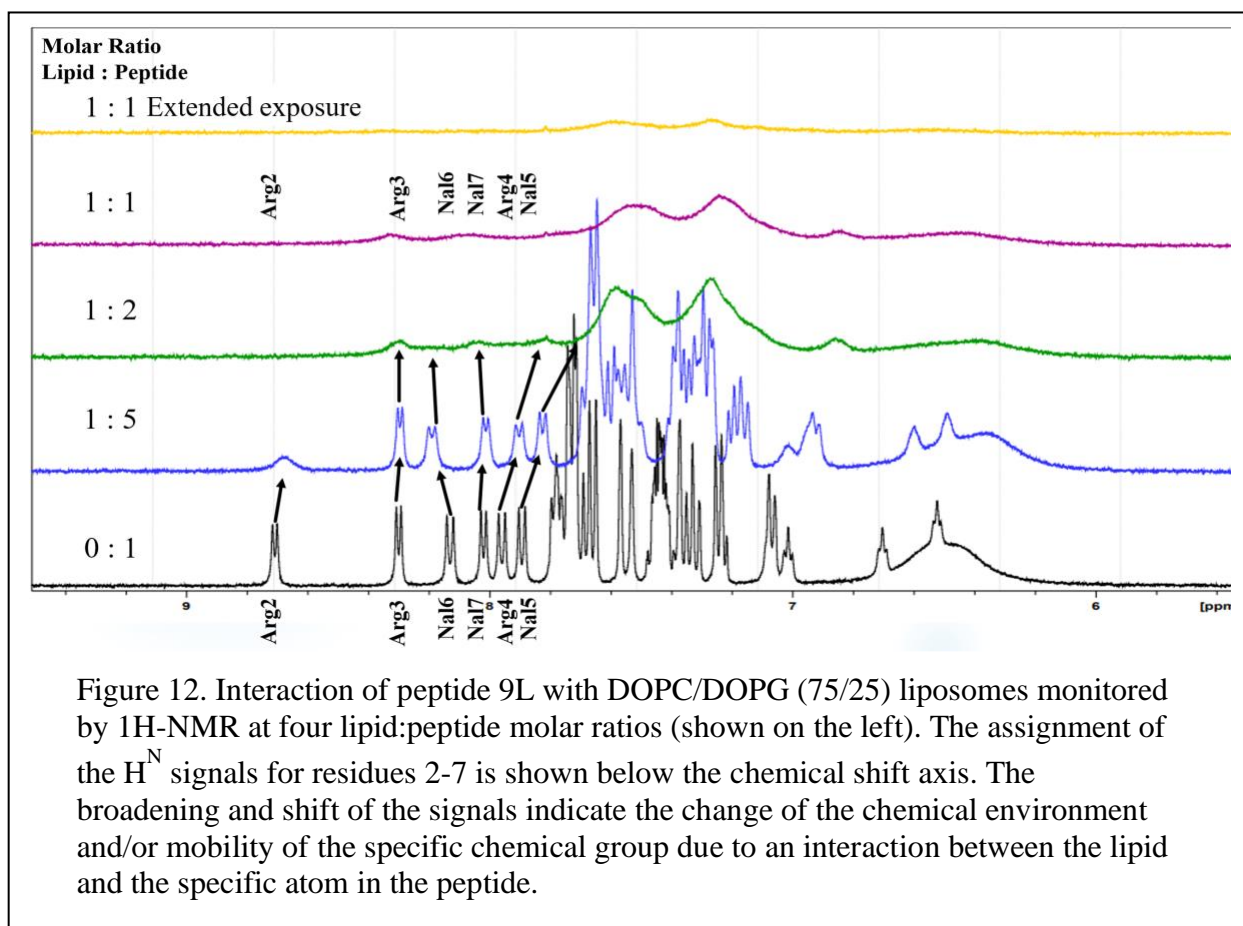
The strip representation in Figure 10 visualizes connections in the NOESY spectrum that show the links between spin systems, allowing sequential assignment of the systems to amino acid residues in the peptide. Chemical shifts of the peptides are summarized in Table 1.

Table 1. Chemical shifts of peptides 8L and 9L in water at 25 °C						
8L	HN	HA	HB	HG	HD	HE
R1	-	4.135	1.729	1.995	3.280	7.283
R2	8.881	4.433	1.714	1.859	3.259	7.249
R3	8.594	4.291	1.623	1.733	3.272	7.290
R4	8.162	4.140	1.383	1.443	3.132	7.164
Dip5	8.238	5.142	4.290	-	-	-
Dip6	8.478	5.076	4.356	-	-	-
Dip7	8.099	4.717	4.356	-	-	-
9L	HN	HA	HB	HG	HD	HE
R1	-	3.950	1.531	1.801	3.033	7.057
R2	8.682	4.256	1.496	1.645	2.893	6.937
R3	8.313	4.062	1.026, 1.167	1.328	2.441, 2.54	6.616
R4	8.036	4.060	0.830	1.045	2.204, 2.294	6.572
Nal5	7.924	4.575	2.175	-	-	-
Nal6	8.160	4.685	2.805, 2.939	-	-	-
Nal7	8.149	4.689	2.945, 3.236	-	-	-

3.1.2. Peptide-Membrane Interactions

While the strong aggregation of the cyclic peptides prevented detailed analysis of their interactions with the phospholipid bilayer membrane, obtained assignment for the linear peptides allowed us to compare the NMR data of the linear peptides in water and in the presence of lipid vesicles or liposomes. The liposomes composed of zwitterionic (DOPC), and anionic (DOPG) lipids are considered a reasonable model to represent the negatively charged inner bacterial membrane (Sautrey et al., 2015).





Two major characteristics of NMR signals may be affected by a change in sample composition. Changes in the signal linewidth indicate either the change in mobility of the affected chemical group or the possibility of conformational heterogeneity. Changes in the signal positions indicate the change in the chemical environment for a specific chemical group. Interaction of the peptides with the large liposome particles (average diameter of approximately 100 nm) could induce both types of changes – due to a change in mobility of the peptide groups upon interaction with large particles and changes in the environment.

The strong advantage of the NMR method is that we can follow these changes for specific atoms or chemical groups. Thus, in the presence of liposomes, both linear peptides 8L and 9L exhibited a broadening of the backbone amide signal from Arg 2 (Figures 11 and 12), which suggests that the *N*-terminal arginine residues (Arg 1 and Arg 2) are the initial point of

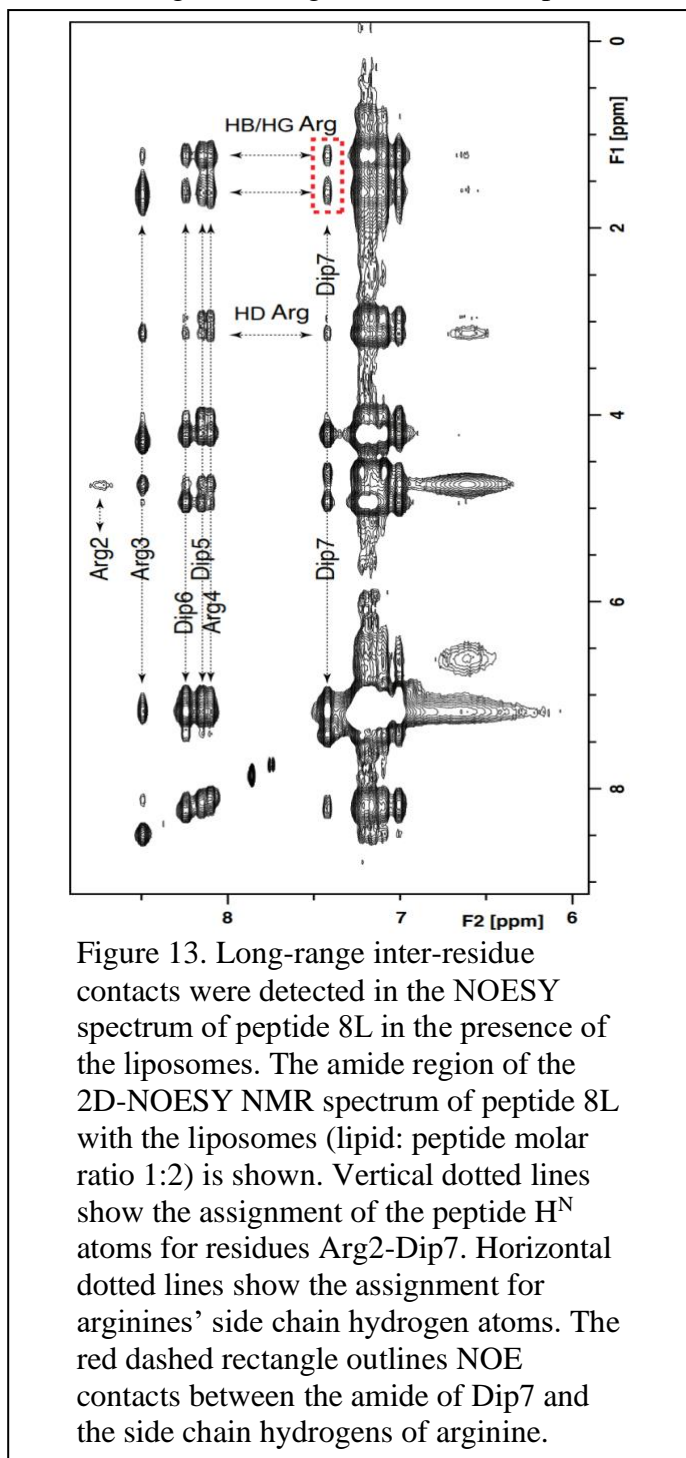
contact with the liposomes at the lipid:

peptide molar ratio of 1:5. As the concentration of the liposomes increased,

at the lipid:peptide ratio of 1:2, the signals of all other backbone amides decreased in intensity and broadened strongly compared to backbone amide signals of the peptides in water (Figures

11 and 12). When the lipid: peptide molar ratio reaches 1:1, all peptide resonances have become severely broadened because of the binding of the peptides to the liposomes. Based on these

observations, we concluded that the initial point of contact of the linear peptides 8L and 9L with the liposome surface are positively charged *N*-terminal arginine residues. In addition, chemical shifts of Dip7 in 8L and Nal5 in 9L give



another insight into the interaction between the liposomes and linear peptides. As the lipid concentration increases, the signals broaden and shift away from the initial position in response to stronger contact with the lipids. These shifts induced by the interaction with the liposome may represent increased structural rigidity and straightening of the peptide. As the peptide moves from hydrophilic to the mixed amphiphilic environment, the atoms in contact with the liposomes demonstrate the chemical shift migration.

NOESY-specific cross-peaks indicate a distance below 6 Å between any atoms. The analysis of 2D-NOESY data of peptide 8L in the presence of liposomes with a lipid: peptide ratio of 1:2 shows a restricted distance (below 4 Å) between amide hydrogen of Dip7 and HB/HG atoms of Arg3 and/or Arg4 (Figure 13). Such close contacts between the backbone, HN of Dip7, and side chains of Arg3 and/or Arg4, are possible only in the linear peptide's compact, ring- or hairpin-like conformation. The absence of these contacts in the NMR spectrum of the peptide sample in water suggests structural changes of the linear peptide 8L upon interaction with the liposomes. In turn, NMR spectra of the peptide 9L with liposomes do not reveal the contacts between C-terminal aromatic residue and arginine, suggesting primarily extended conformation of the peptide 9L in the presence of liposomes.

3.1.3. SAR of Cyclic and Linear Peptides

The cyclic peptides 8C and 9C demonstrated two remarkable distinctions from the linear peptides in their behavior in water and the presence of liposomes. First, the amide hydrogens in both tested cyclic peptides have severely broadened signals as well as produce additional minor signals, potentially due to the presence of several conformers and/or multimers of the peptides in solution with slow (millisecond timescale) exchange between the conformations and/or oligomeric states. Both the signal broadening and the presence of the minor signals can be

explained by the conformational heterogeneity resulting from a strong tendency to form high-order oligomers at peptide concentrations above 0.5 mM.

The second distinction is a simultaneous broadening of all amide hydrogen signals upon adding the lipids, supposedly due to the restrained mobility of the cyclic backbones after initial anchoring on the liposome surface. Peptides or narrow signals from the backbone amides, which potentially correspond to more mobile conformers or low-order oligomers or monomers of the peptides, disappeared at the lowest lipid/peptide molar ratio of 1:5.

The results of NMR experiments with the linear and cyclic peptides in water in the presence of the liposomes were used in further computational analysis of the peptide's behavior in different media. Particularly, molecular dynamics simulations corroborated NMR data that the linear peptides 8L and 9L in water are primarily unstructured and very flexible. These peptides adapt their structure to match the membrane bilayer's hydrophilic and hydrophobic regions upon interaction with the lipid bilayer. Probably due to the flexibility of the peptides, this matching process does not result in substantial disturbance and deformation of the membrane bilayer, which explains the low antibacterial activity of the linear peptides 8L and 9L. The cyclic peptides 8C and 9C do not change their structure substantially when transitioning from water to the lipid bilayer.

The compact ring structure of the cyclic peptides with well-defined cationic and hydrophobic areas of the molecular surface requires the lipid bilayer to adapt to the incorporated rigid amphiphilic molecules, thus causing disbalance in the distribution of lipids in the bilayer, weakening lipid-lipid interactions, and destabilizing the membrane. It should be noted that the balance between the charge and hydrophobicity, as well as the distribution of charged/hydrophobic areas on the peptide surface, along with other structural features, are also

extremely important for the efficiency of peptide-membrane interaction, behavior, and membrane action of the peptides.

3.2. Spatial Structure of the Peptide HP2

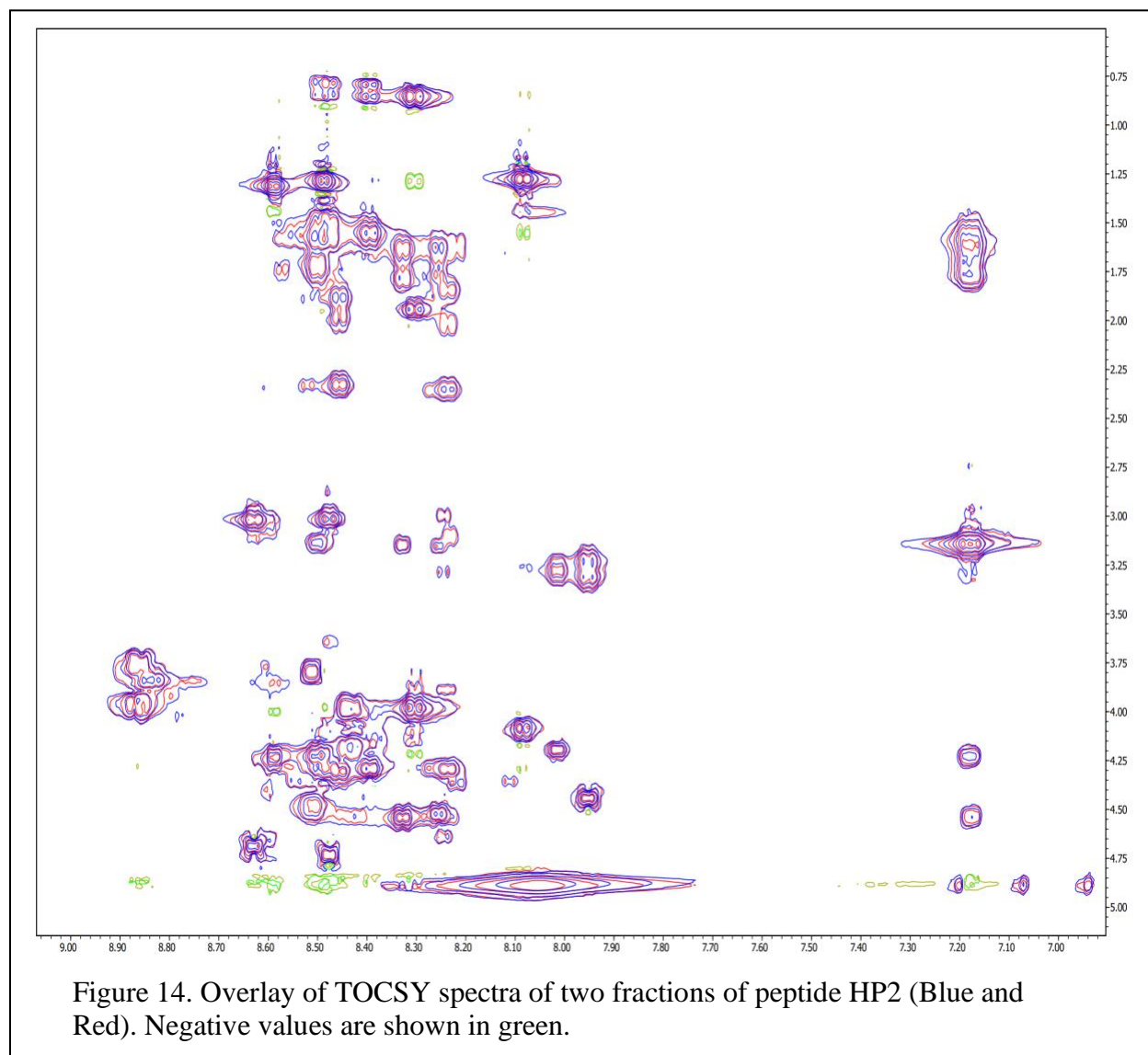
The peptide HP2, selected for structural study and analysis, has been designed to block NEMO's interaction with HOIP, which is important for activating NF- κ B. The synthetic peptide was designed to mimic the structure of the HOIP NZF1 region (Table 2), which, according to the X-ray structure (PDB ID 4OWF, <https://www.rcsb.org/structure/4OWF>), directly interacts with NEMO.

Table 2. Amino acid sequences of the peptide HP2 and the corresponding region of HOIP	
Synthetic peptide	AAAVLCGPGCERPRLA
HOIP	³⁶⁰ TFENE ³⁶⁵ AAAVLCS-ICERPRLA ³⁷⁹ QPPSL ³⁸⁴

3.2.1. Preliminary NMR Analysis

The peptide has been produced, purified, and prepared for structural study and analysis in Dr. Rahighi's lab. During the purification of the peptide with reverse-phase HPLC, two fractions of the peptide HP2 were collected at two different elution points, assuming a difference in the overall hydrophobicity of the molecules. The products in both fractions have the same molecular weight according to MALDI MS analysis.

For the NMR analysis, the samples with both fractions were prepared in identical conditions (see Methods). The two samples, prepared from different HPLC fractions, were compared using 2D-NMR methods. As shown in the overlay of TOCSY spectra for both fractions, every aspect of the spectra: positions, intensities, and shape of the cross-peaks, are identical in the samples (Figure 14). Based on this analysis, we concluded that the fractions were identical in chemical composition. However, it asks what caused the change in the peptide hydrophobicity in these fractions. Hence, we addressed this question during a further closer analysis of the NMR data.



3.2.2. NMR Assignment

In NMR spectra of a peptide, one should expect the number of spin systems originating from the H^N atoms to be equal to the number of amino acids less one (N-terminal residue) and the number of proline amino acid residues (that do not have the H^N atom). Thus, for HP2, we should expect 13 spin systems (16 amino acids less N-terminal A1 and two prolines, P8 and P13) in the H^N region of TOCSY spectra. However, as shown in Figure 15, we identified 19 H^N -originated spin systems.

Upon completion of finding all the systems, 21 total spin systems were accounted for when there should only be 13 backbone and 2 Arg side chains total (one unique spin system per amino acid residue). Since the chemical identity and purity of the peptide were confirmed, the most probable explanation of the additional spin systems is a conformational heterogeneity of the peptide, specifically, the presence of more than one stable conformation with a slow in NMR

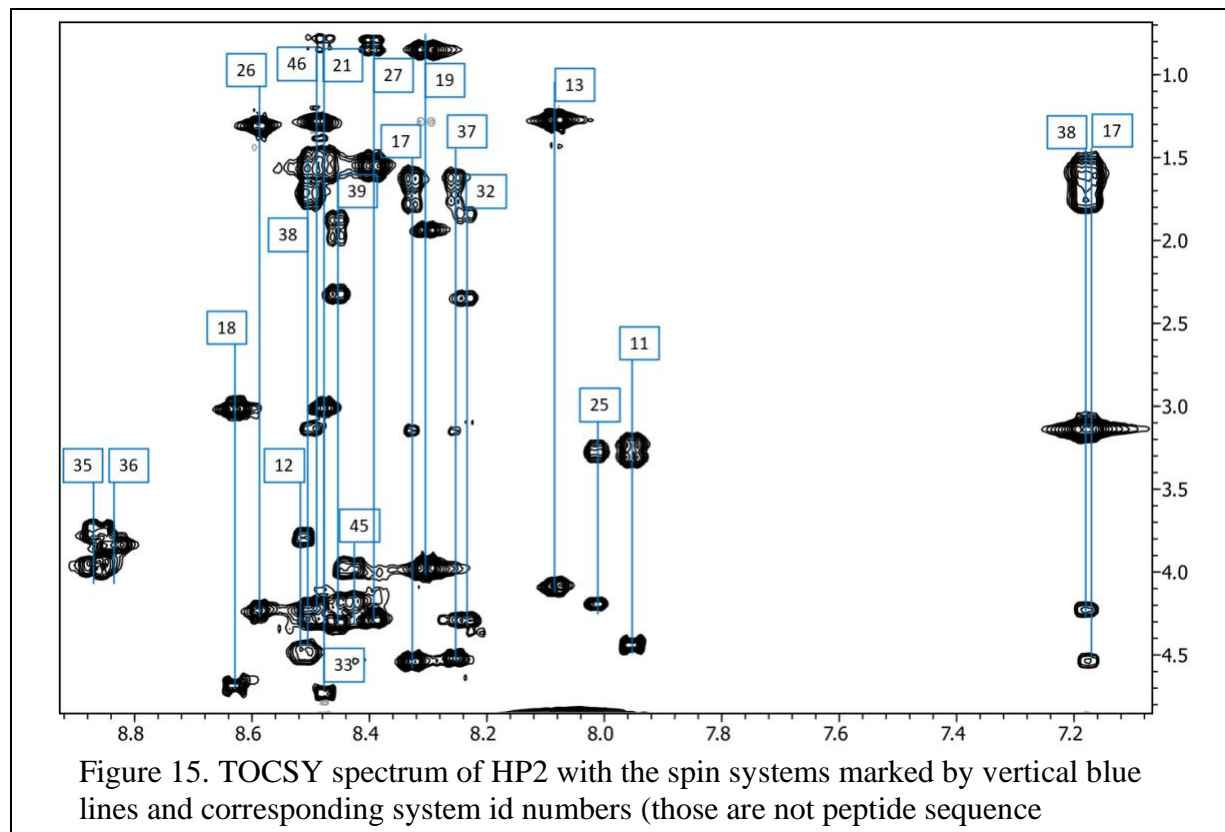
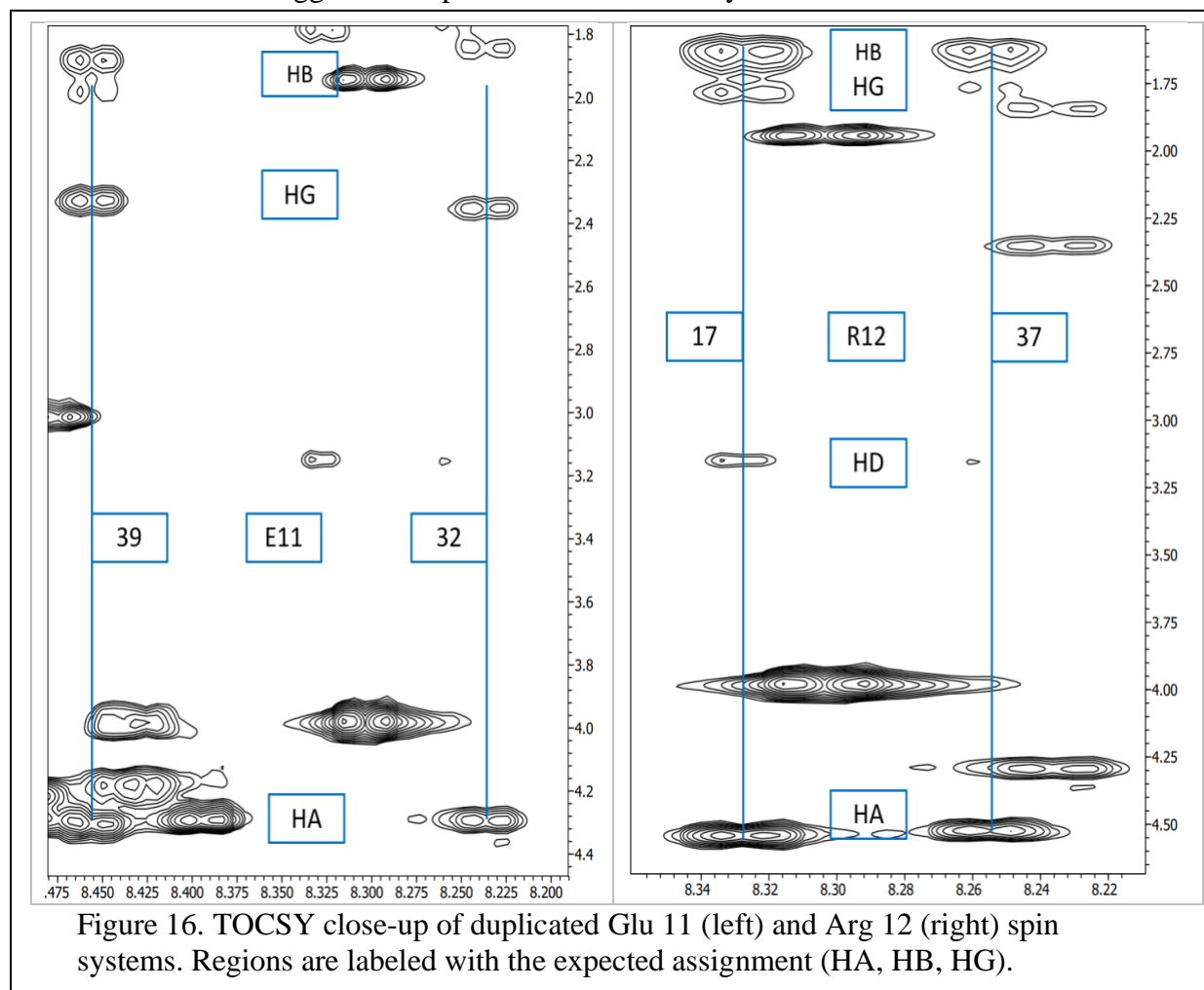


Figure 15. TOCSY spectrum of HP2 with the spin systems marked by vertical blue lines and corresponding system id numbers (those are not peptide sequence)

timescale (lifetime of the conformers is hundreds of milliseconds or more) exchange between different conformers.

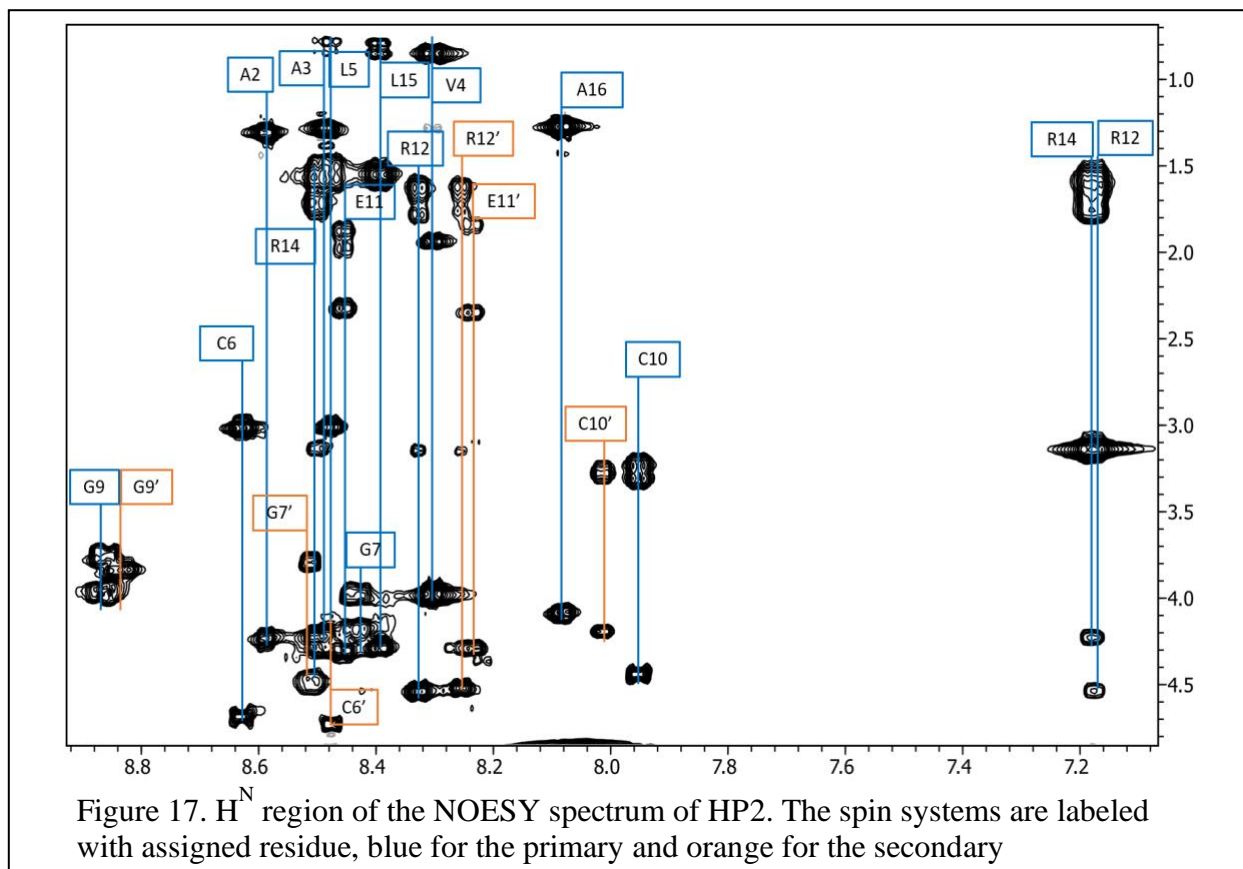
Analysis of the identified spin systems shows that they can be arranged in pairs with substantially different chemical shifts for the H^N atom and much less difference for the other atoms in the systems (Figure 16). Also, the corresponding cross-peaks in the paired systems exhibited a similar distribution of intensities. For example, cross-peaks in System 17 match cross-peaks in System 37, and System 39 matches System 32. In total, seven pairs of spin systems were identified. The summary of paired spin systems with the assignment to their amino acid types is provided in Table 3. The evidence of doubled spin systems for at least 7 out of 16 amino acid residues suggested the presence of a secondary conformation.

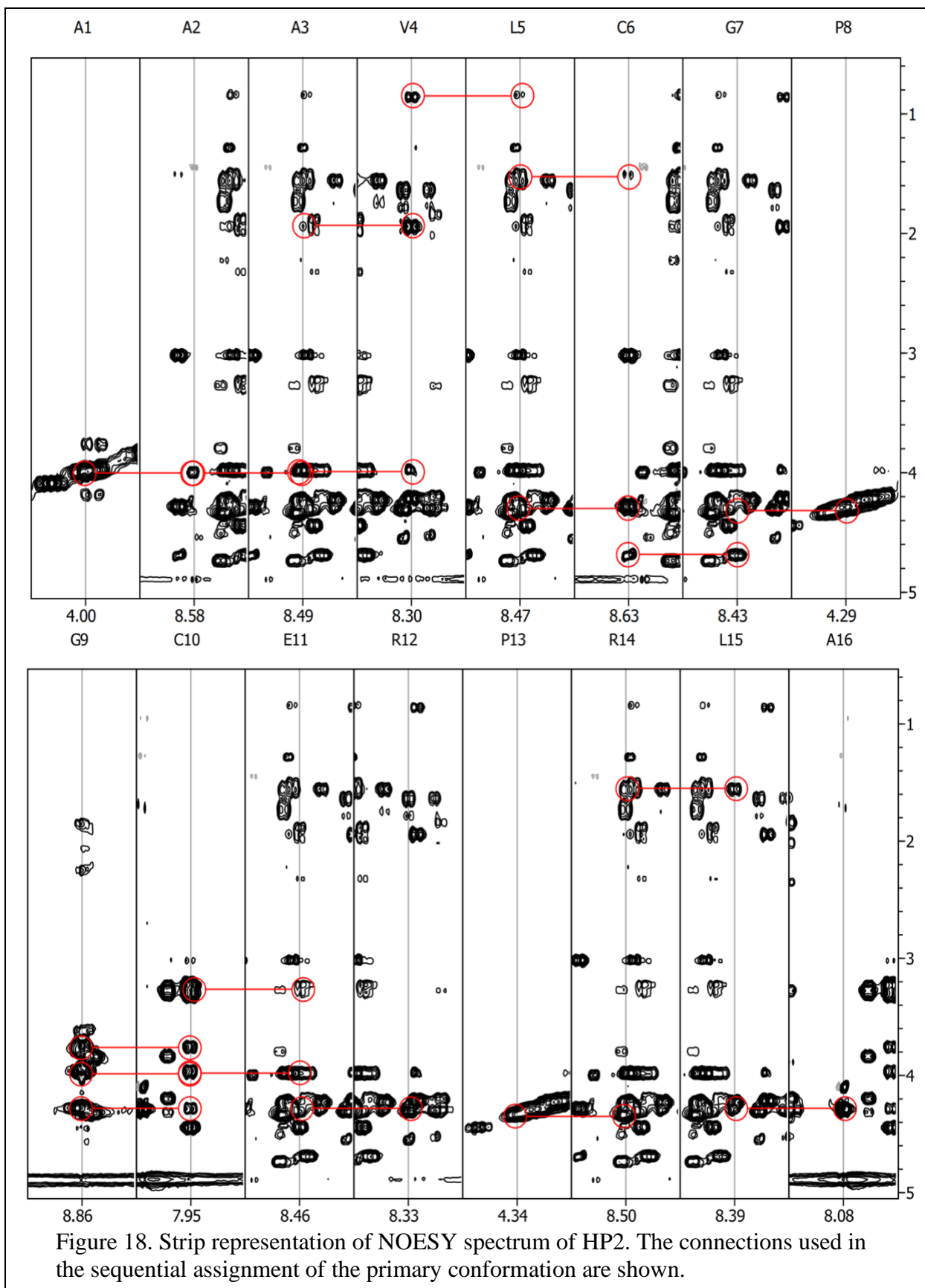


The regions demonstrating conformational heterogeneity were identified during the sequential assignment. The basis for the heterogeneity and the difference between the conformers were revealed and confirmed at the structure calculation stage. Our preliminary analysis of the NMR data indicated that the possible cause of the conformational heterogeneity could be the cis-trans isomerization of proline peptide bonds, as these bonds may have a low energy barrier for isomerization in short peptides.

The peptide contains two prolines (8 and 13). Since the duplicated NMR signals were found only for C6, G7, P8, G9, C10, E11, and R12 (Figure 17), the cis-trans isomerization of P8 is the most likely cause of conformational flexibility.

Analysis of the NOESY-specific cross-peaks (Figure 18) allows us to connect the spin systems and complete the sequential assignment for both primary and secondary conformers (Table 3).





HP 2	HN	HA	HB	HG	HD	HE
A1	-	4.001	1.450	-	-	-
A2	8.585	4.233	1.312	-	-	-
A3	8.487	4.222	1.285	-	-	-
V4	8.304	3.983	1.942	0.854, 0.854	-	-
L5	8.475	4.290	1.508, 1.582	1.508	0.785, 0.785	-
C6	8.627	4.688	3.020, 3.020	-	-	-
C6'	8.476	4.734	3.017, 3.017	-	-	-
G7	8.432	3.989, 4.177	-	-	-	-
G7'	8.507	3.794, 4.482	-	-	-	-
P8	-	4.285	1.859, 1.950	2.058, 2.240	3.617	-
P8'	-	4.325	1.870, 1.870	2.058, 2.240	3.600	-
G9	8.862	3.757, 3.972	-	-	-	-
G9'	8.835	3.831	-	-	-	-
C10	7.949	4.443	3.242, 3.307	-	-	-
C10'	8.015	4.196	3.280, 3.280	-	-	-
E11	8.456	4.303	1.882, 1.983	2.327, 2.327	-	-
E11'	8.237	4.294	1.842, 2.013	2.353, 2.353	-	-
R12	8.328	4.536	1.631, 1.631	1.790, 1.790	3.167	7.175
R12'	8.254	4.525	1.625, 1.625	1.765, 1.765	3.153	7.175
P13	-	4.336	1.785, 1.944	2.229, 2.229	3.557, 3.742	
R14	8.499	4.235	1.576, 1.576	1.715, 1.715	3.132	7.181
L15	8.395	4.294	1.554, 1.554	1.496	0.793, 0.856	-
A16	8.804	4.101	1.276	-	-	-

3.2.3. Structure Calculation and Analysis

After the two sets of cross-peaks were identified in the NOESY spectrum for primary and secondary conformers, the cumulative NOESY data were converted to peak lists and prepared for integration. The diagonal and degenerate peaks were vetted out. As described in the Methods, a stand-alone model peak tuned the parameters for model-based linear fit integration.

The NOESY cross-peak volumes were also used to generate an alternative set of structural restraints. The cross-peak data were split into three groups: (1) for the structurally uniform part of the peptide (residues 1-5 and 13-16), (2) for the primary, and (3) for the

secondary conformers in regions 6-12. These sets were processed separately to calculate the distance restraints because the conformers have different populations in the solution and different contributions to the NOE intensities.

All peptide molecules contribute to the same dataset for regions 1-5 and 13-16, where a single conformation was detected. However, different populations of the peptide molecules contribute to the different conformations in regions 6-12. NOE intensities are proportional to the concentration of the molecules contributing to the signal; therefore, we calculated the interatomic distance restraints for each subset of the data separately.

Finally, the generated restraints were combined into two large datasets of distance restraints – one for the primary and another for the secondary conformers. The summary of NOE restraints for both conformers is provided in Tables 4 and 5.

The structural data for primary and secondary conformers were used separately by the CYANA program to calculate 100 structures starting from random conformations. The 20 best structures of each set with the lowest target function (representing a summary of violations of the experimental and non-experimental constraints) were analyzed to identify consistent violations of the experimental constraints. After the refinement of the input sets of the restraints, the final sets of 100 structures were calculated, and the set's 20 best structures for the primary and the structure analysis with CHIMERA used secondary conformations (Tables 4 and 5).

A comparison of the primary and secondary structure sets shows that the Primary conformations have lower values for the violations and penalty function due to the higher number of experimental constraints. Indeed, the primary data set includes 70 distance constraints in regions 5-11, while the secondary data set has only 35 constraints. Having more constraints leads to lower violations and a better-defined structure.

Upon refinement of the models, the file with coordinates of atoms (pdf format) for the best 20 structures was generated by Cyana, and its PDB file was used in CHIMERA (UCSF) software to analyze the 3D structures visually. The obtained spatial structures of the peptide are also compared with the X-ray structure of the NEMO-HOIP complex.

Table 4. Statistic for the best 20 structures calculated for the Primary conformation			
Parameter	Quantity	Unit	Value
Target function	Average \pm rms	\AA^2	0.0481 \pm 0.0248
Number of distance constraints	NOE	Fixed/Flexible	61/70
	Disulfide Bridge	-	3
	Hydrogen bond	-	0
Upper constraints limits	RMS \pm S.D.	\AA	0.0097 \pm 0.0032
Lower constraints limits	RMS \pm deviation	\AA	0.0006 \pm 0.0023
Van der Waals distance limits	Sum \pm deviation	\AA	0.3 \pm 0.1
Average rmsd to mean for residues 5 to 11	Backbone	\AA	0.37 +/- 0.27
	Heavy atom	\AA	0.62 +/- 0.27

Table 5. Statistic for the best 20 structures calculated for the Secondary conformation			
Parameter	Quantity	Unit	Value
Target function	Average \pm rms	\AA^2	0.0783 \pm 0.0442
Number of distance constraints	NOE	Fixed/Flexible	61/35
	Disulfide Bridge	-	3
	Hydrogen bond	-	0
Upper constraints limits	RMS \pm S.D.	\AA	0.0138 \pm 0.0049
Lower constraints limits	RMS \pm S.D.	\AA	0.005 \pm 0.0118
Van der Waals Function	Sum \pm S.D.	\AA	0.3 \pm 0.08
Average rmsd to mean for residues 5 to 11	Backbone	\AA	0.96 +/- 0.40
	Heavy atom	\AA	1.84 +/- 0.50

3.2.4. Conformational Heterogeneity of HP2

As discussed, calculating HP2 structure in solution based on NMR data shows two distinct conformations. The basis of the conformational heterogeneity is the cis/trans isomerization of the Gly7-Pro8 peptide bond. The peptide bond of prolines can switch between cis and trans isomers

because of similar energy levels for the *cis* and *trans* isomers and a relatively high energy barrier to switch between the conformers. In most cases, other amino acid residues adopt the *trans* isomer conformation, mainly due to the less steric repulsion of amide hydrogen to the preceding C_{α} atom than the following C_{α} . Since proline does not have amide hydrogen, the energy levels in *trans* and *cis* conformations are comparable, while the transition barrier is higher (approximately 12 Kcal/mol).

The type of the preceding residue also influences the energy levels and, thus, the population of the *cis* isomer. For most amino acid residues preceding proline, the population of *cis*-proline isomers is typically 3-10% (Alderson et al., 2017). When the preceding amino acids are glycine

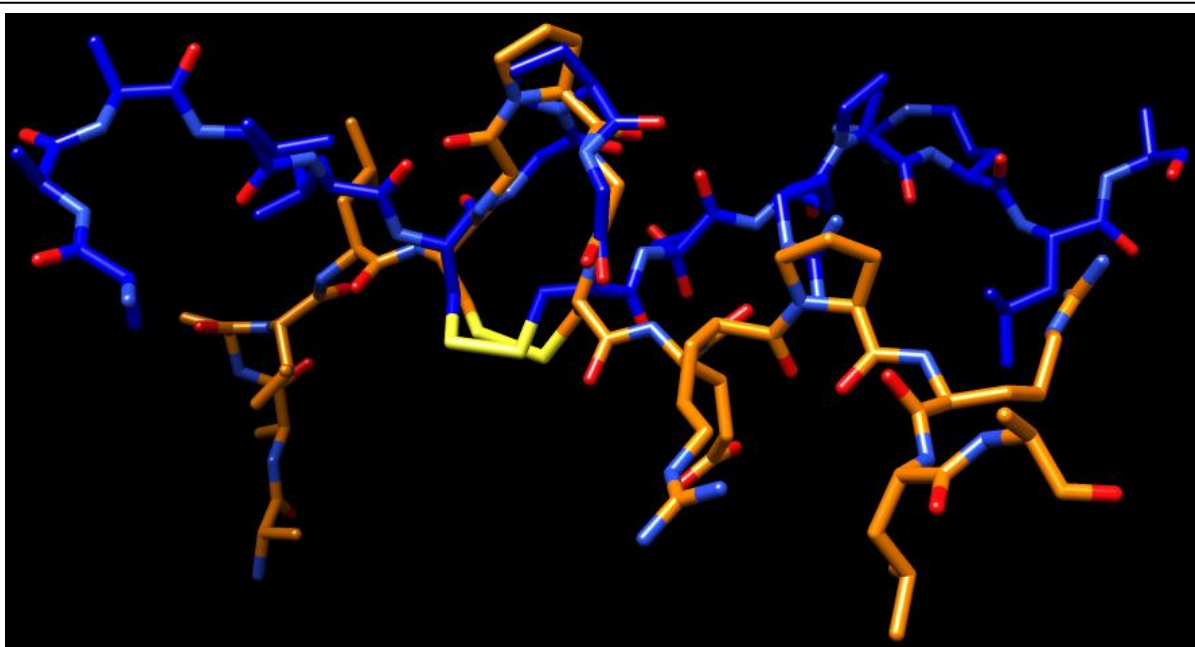


Figure 19. Superposition of the best structures from the primary (blue) and secondary (orange) conformations sets. The structures are superimposed by coordinates of backbone atoms of regions 5-11.

(Sarkar et al., 1984) or aromatic residue, the *cis*-isomer population of proline may increase up to 40% (Gustafson et al., 2017).

The relative population or, in other words, the molar ratio of the *cis* and *trans* conformers can be estimated using the intensities of NOE cross-peaks originating from the same atoms in

different conformers. Thus, we found that the ratio between primary and secondary conformers for HP2 is approximately 63% (trans) to 37% (cis).

The comparison of both conformations (Figure 19) shows slight differences in the spatial structure of the Cys6-Cys10 loop, which contains isomeric Pro8 residue. The rmsd between the best primary and secondary conformations for the backbone atoms of the 6-10 region is 0.76 Å

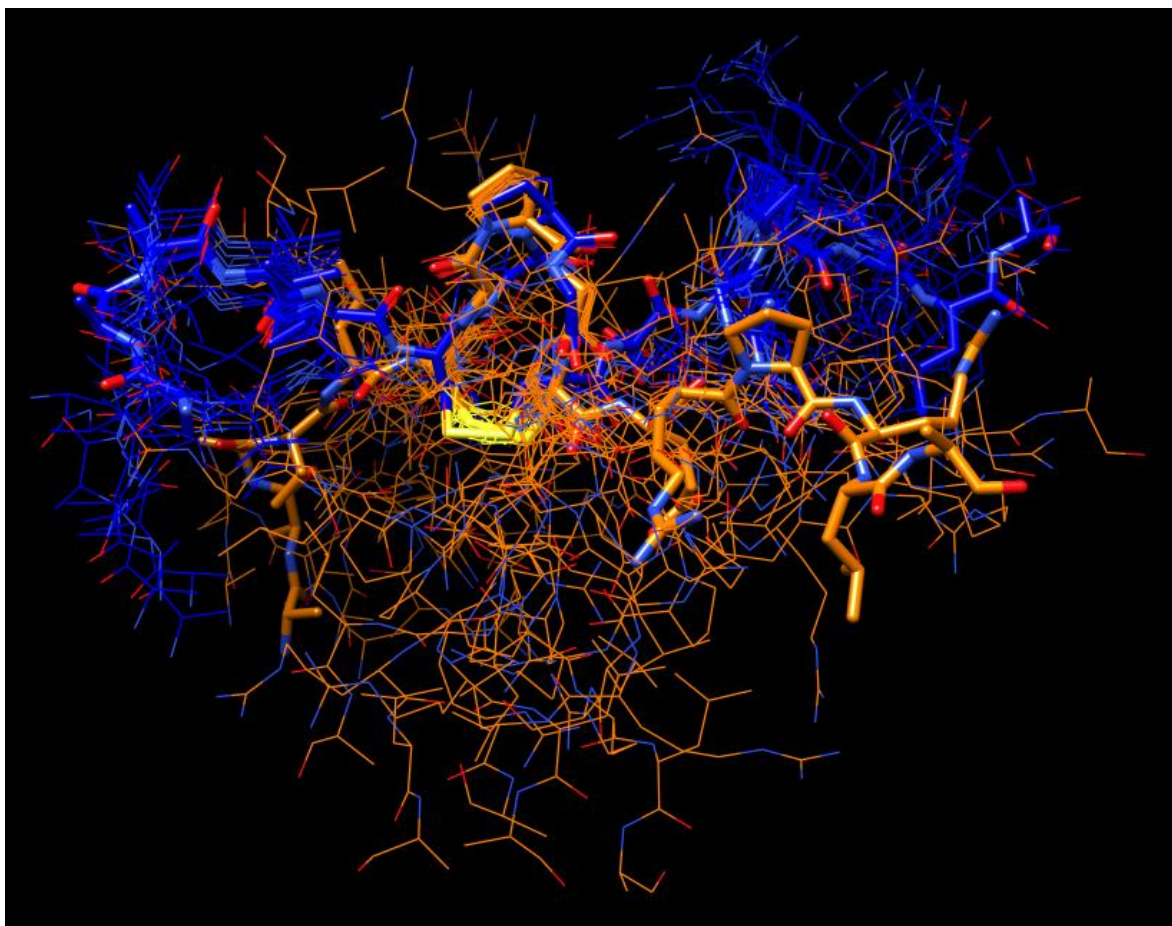


Figure 20. Best HP2 structures of primary (blue) and secondary (orange) conformation. The 20 best structures for each conformer are superimposed using coordinates of region 5-11 backbone atoms. The structures with the lowest overall violations in both sets are shown with thick bonds.

and mostly reflects the difference between the cis and trans orientations of the Pro8. The disulfide bridge between Cys 6 and Cys 10 provides additional restriction on the spatial structure of this region, thus making the conformation of the 6-10 region relatively similar in both forms.

The conformers' N- and C- termini show diverse structural arrangements (Figure 20). Not only the N- and C- termini of the conformers are facing different directions, but their structural characteristics within each group also differ, which we discuss below.

The primary conformation (Figure 21) has well-ordered backbone conformation for residues 5-11 (rmsd to the mean structure is 0.37 ± 0.27 Å). N- and C- terminal regions (residues 1-4 and 12-16) are more flexible (Figure 21) but still demonstrate uniform orientations relative to the central loop Cys6-Cys10.

The sufficient number of experimental constraints used in the calculation (Table 4) allows

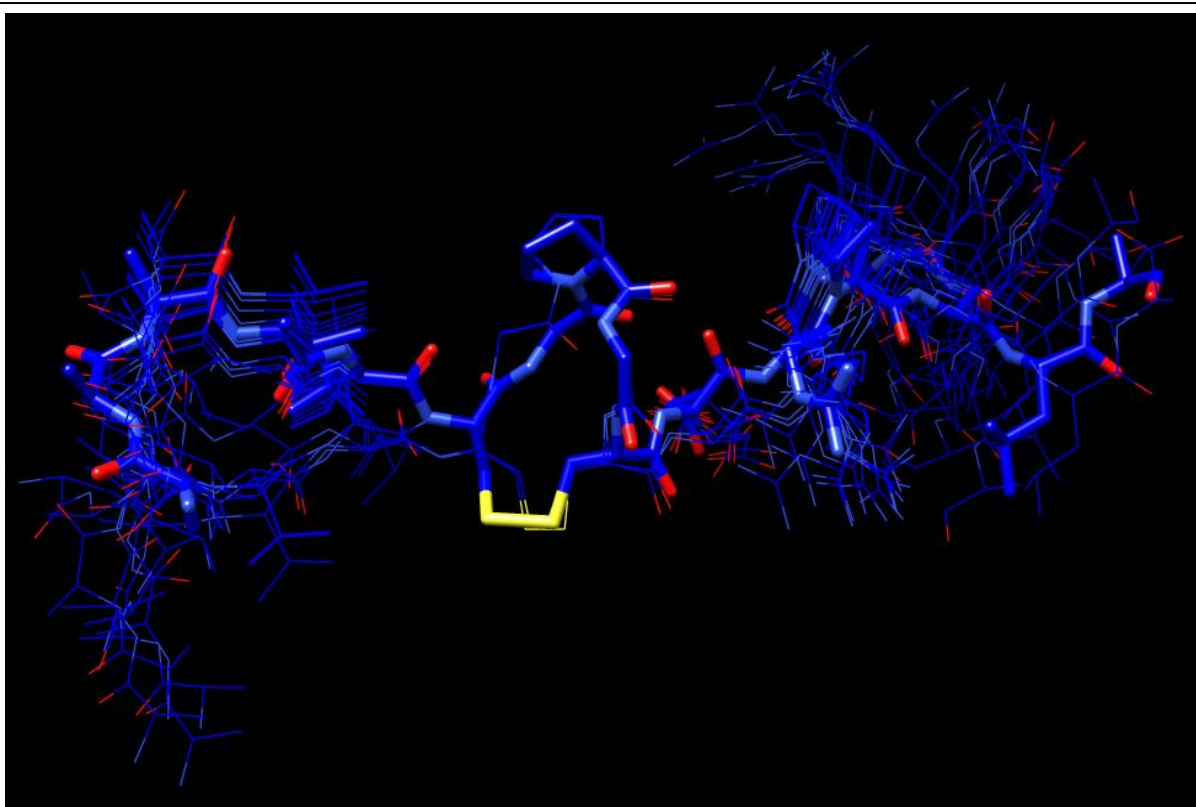


Figure 21. 20 Best HP2 structures of primary conformation. Structures are superimposed using coordinates of backbone atoms on regions 5-11. The structure with the lowest overall violations is shown with thick bonds.

us to identify in general localization of the flexible terminal regions. For these regions composed of 9 residues, we obtained 70 meaningful distance constraints, which is usually enough for structure calculation (Clare et al., 1993). However, since most of these constraints are short-

range, i.e., within the same amino acid residue or between neighboring residues in the sequence, they need to provide more information to define the secondary structure of the backbone. The absence of long-range distance constraints (i.e., constraints between atoms in sequentially distant residues) indicates a flexible structure.

The secondary conformation (Figure 22) has a relatively ordered backbone structure in the central loop (residues Cys6-Cys10), similar to the primary conformation (Figure 21). However,

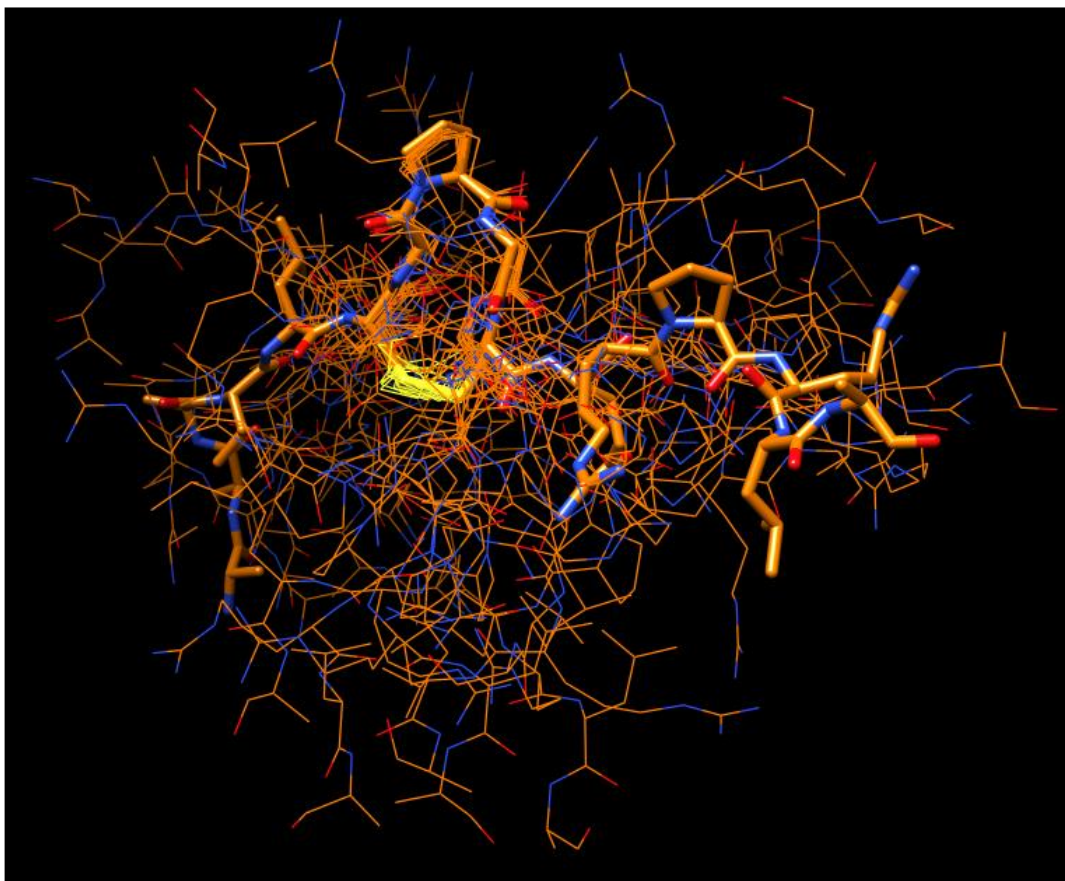
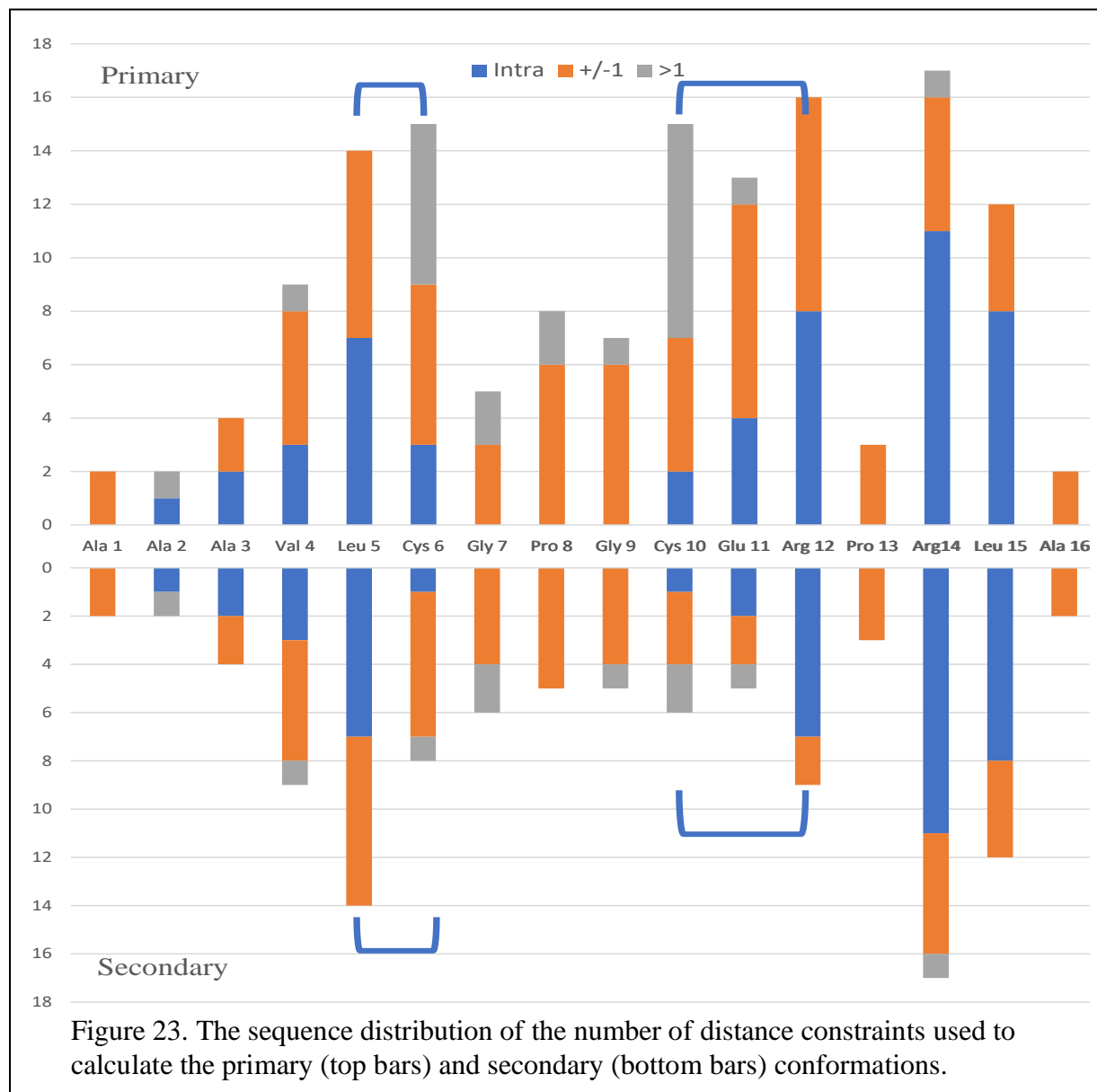


Figure 22. 20 Best HP2 structures of secondary conformation. Structures are superimposed using coordinates of backbone atoms on regions 5-11. The structure with the lowest overall violations is shown with thick bonds.

due to a lower number of distance constraints (35 vs. 70), the spatial structure of the loop is less defined in the secondary conformation. Residues 5-11 have much higher backbone rmsd (0.96 ± 0.40 , Table 5) than the primary conformation (0.37 ± 0.27 , Table 4).

Compared to the primary conformation, N- and C- terminal regions (residues 1-5 and 11-16) in the secondary conformation are more flexible and dispersed in conformational space (Figure 22). Analysis of the pool of distance constraints (intra-residue, neighboring, or inter-residue) aids in understanding why the secondary conformation of the peptide has much more



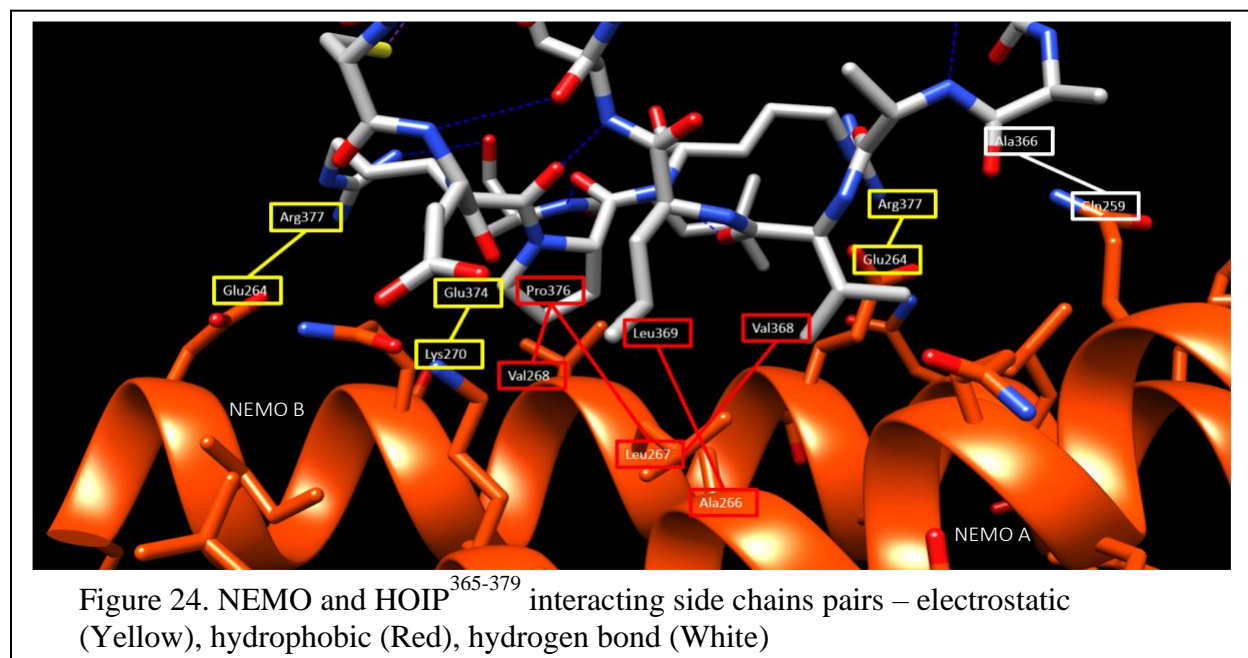
disordered N- and C-termini. Regions Ala 1 to Val 4 and Arg 14 to Ala 16 have the same distance constraints in primary and secondary conformations. Thus, their local structures are the

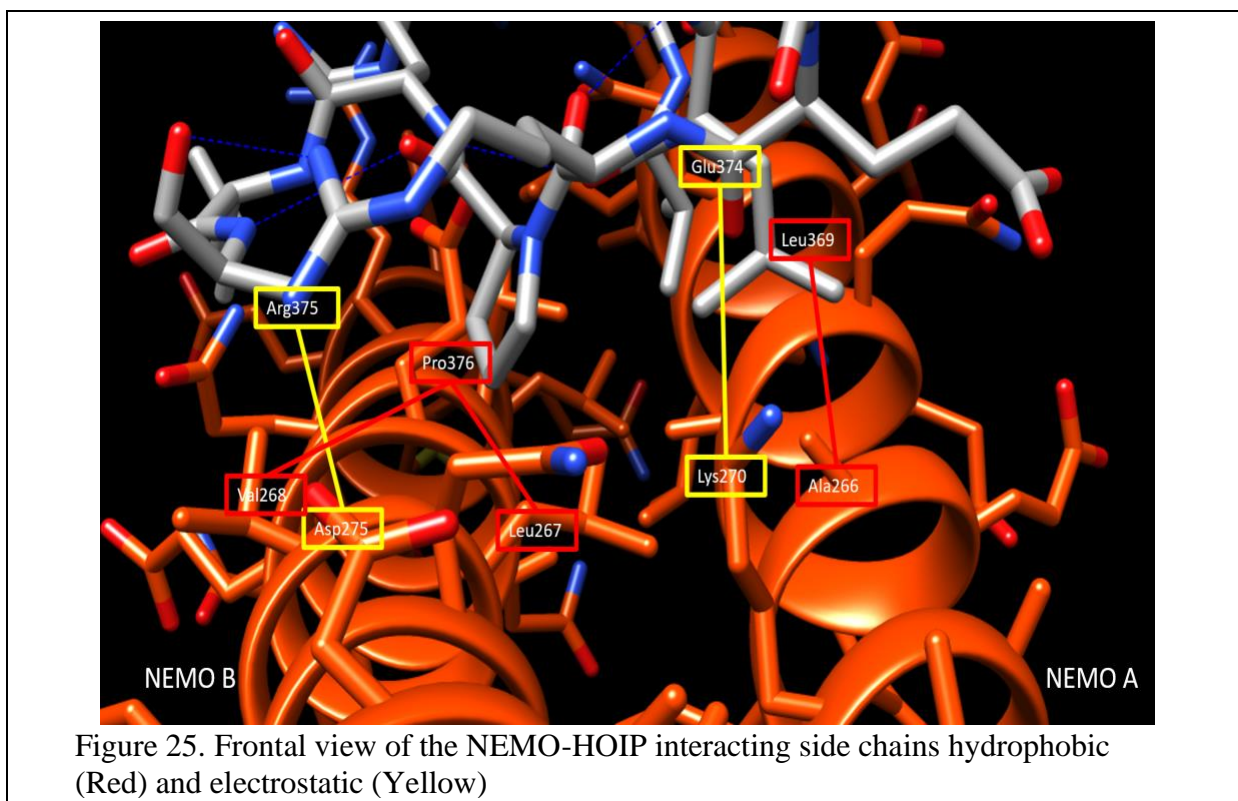
Same in both forms. However, there is a difference between the number of distance constraints for Leu 5, Cys 6, Cys 10, Gln 11, and Arg 12 (Figure 23). For these residues in the “hinge regions, “the intra, +/- 1, and >1 constraint is much higher in the primary conformation. The additional constraints in the hinge regions Leu5-Cys6 and Cys10-Arg12 result in more restricted structures of N- and C-terminal regions in primary conformation (Figure 21) and more restricted overall structures of the peptide compared to the secondary conformation (Figures 20 and 22).

In conclusion, our structural analysis shows that HP2 peptide is very flexible in solution. Comparing the HP2 solution structure with the structure of the HOIP NZF1 region in a complex with NEMO helps us assess the effect of HP2 flexibility on the interaction with its target.

3.2.5. Structure of HP2 in Comparison with HOIP NZF1

The primary and secondary conformations are then compared to the X-ray structure of HOIP fragment 365-379 in a complex with NEMO (PDB:4OWF). First, we analyzed the X-ray structure using the Chimera program to identify the side chain responsible for the interaction





between HOIP and NEMO. Residues Ala366, Val368, Leu369, Glu374, Arg375, Pro376, and Arg377 of HOIP have side-chain interactions (hydrophobic, electrostatic, or hydrogen bond) with NEMO side chains (Table 6, Figure 24, Figure 25).

The core of the contact area is formed by hydrophobic side chains of HOIP (Ala366, Val368, Leu369, and Pro376) that are aligned with the hydrophobic cavity between the interacting helices of NEMO (Figure 25, Figure 26), while the electrostatic and hydrogen bond contacts are shielding the hydrophobic core from the solvent. To create a surface that matches the NEMO surface, the NZF1 domain of HOIP needs to be arranged in a compact structure coordinated with the Zn^{2+} ion (Figure 27). Apart from the Zinc ion, the structure of NEMO-NZF1 is stabilized by several hydrogen bonds, which stabilize the “fingers” with four Cysteine side chains around the Zn^{2+} ion. Thus, in contrast to the structure of HP peptide, HOIP NZF1 structure in complex with NEMO is very well organized.

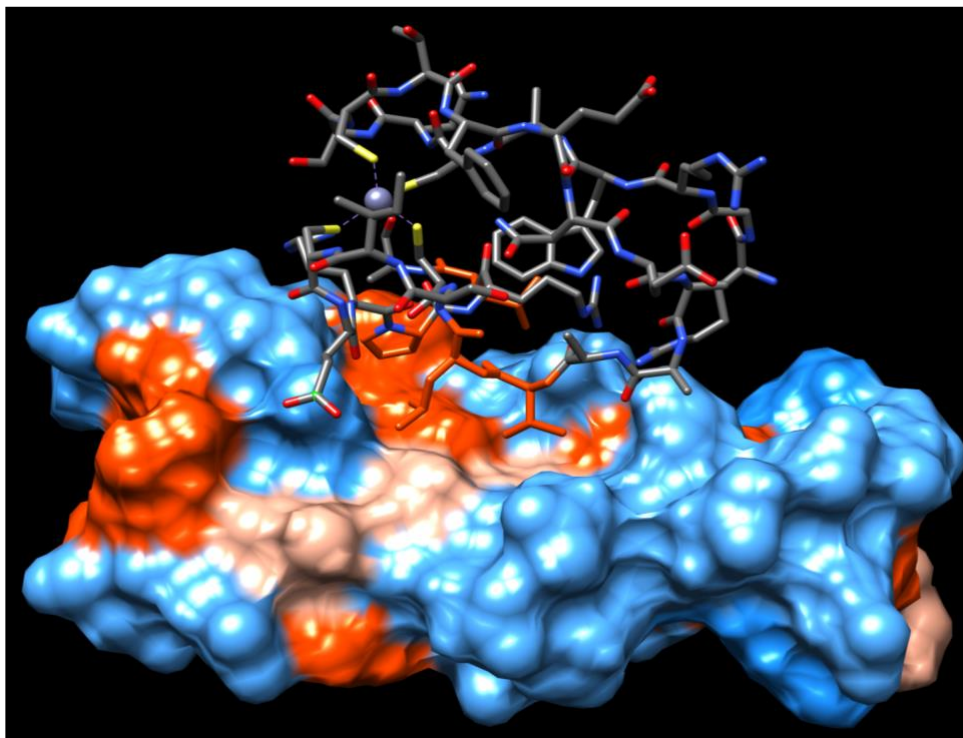


Figure 26. NZF1 domain of HOIP orientation on NEMO hydrophobicity surface (Orange – hydrophobic, Blue – hydrophilic). Hydrophobic side chains of HOIP (Leu369, Val368, Pro376) are shown in Red.

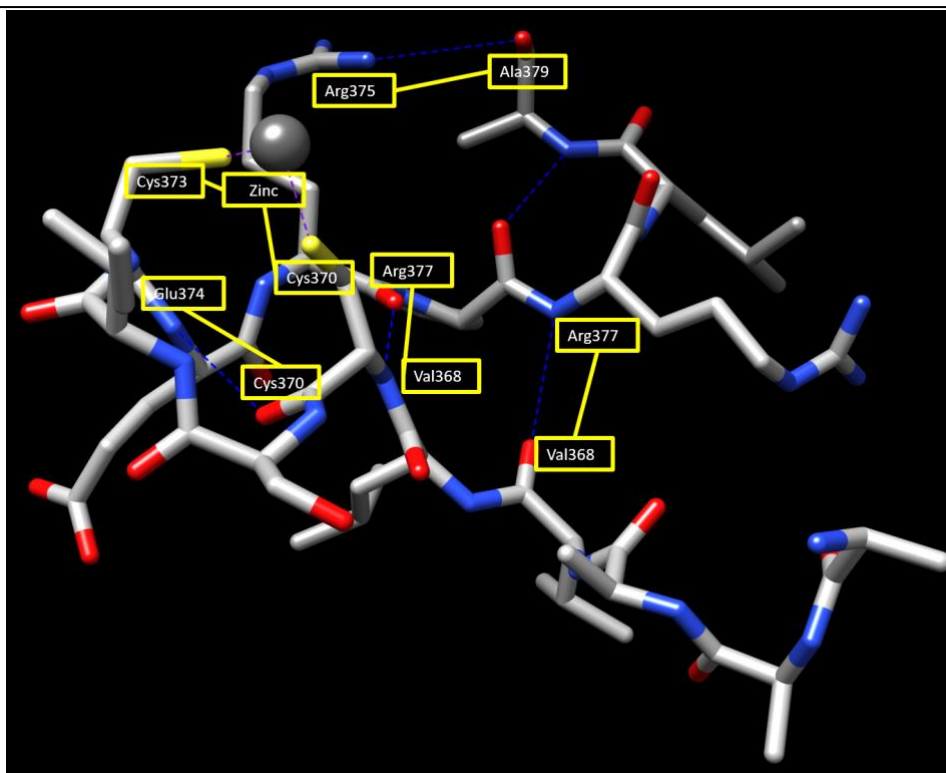


Figure 27. Interactions within HOIP³⁶⁵⁻³⁷⁹ that stabilize the conformation of NZF1 domain.

Despite the addition of the disulfide bonds, peptide HP's primary and secondary structures are unstable and quite different from the X-ray structure of HOIP-NZF1 (Figures 20, 28). Due to the lack of long-range interactions beyond the peptide central loop (Cys6-Cys10), the N- and C-termini of the peptide are not constrained and face different directions than in HOIP NZF1. The peptide termini are often too close to or crashing with the NEMO if the peptide structure is aligned with the HOIP NZF1 structure by the central loop Cys6-Cys10 (Figure 28).

As a result, both peptide conformations cannot recreate the stable surface that will match the NEMO-HOIP interface. Instead, additional cis-trans isomerization of the central loop in the peptide provides additional flexibility to the potential interaction surface. The lack of a well-defined and stable interaction surface in the peptide and added flexibility of the backbone make it impossible to

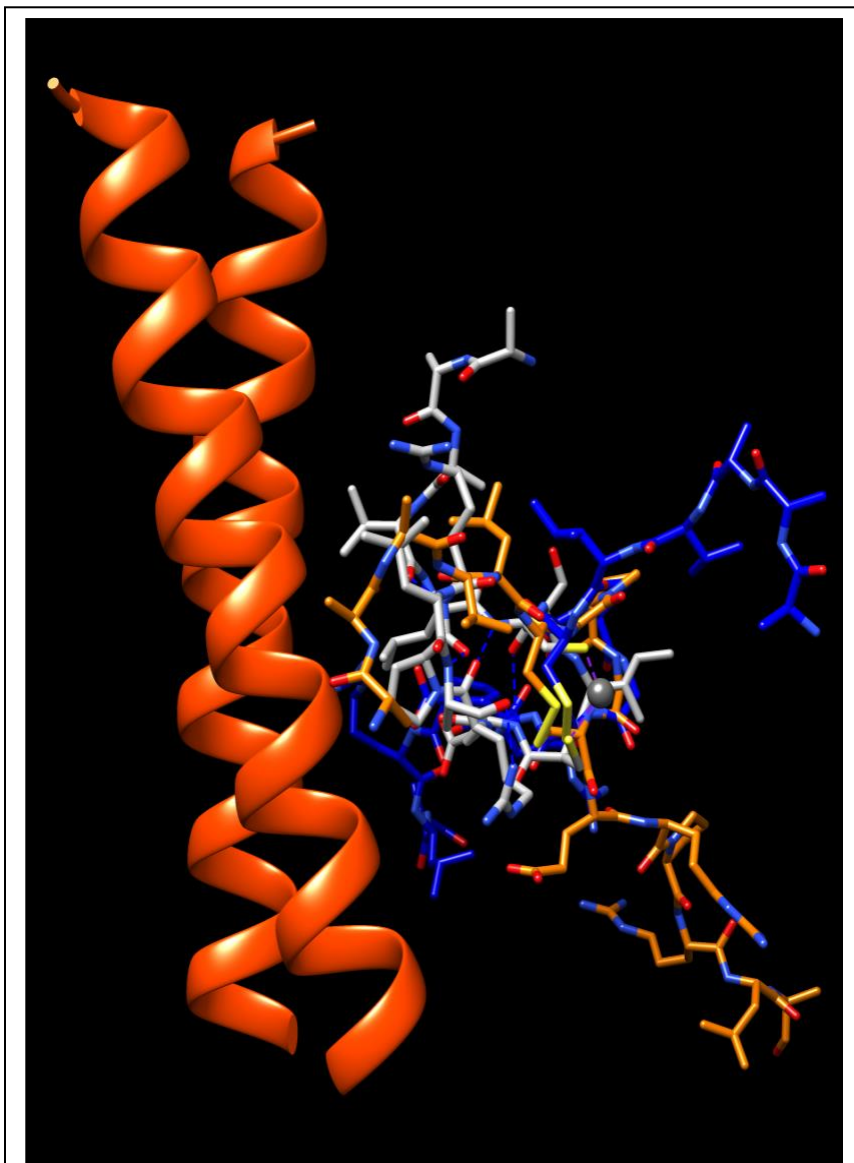


Figure 28. Primary and secondary conformation of peptide HP2 aligned to HOIP structure next to NEMO.

mimic the structural characteristics of HOIP-NFZ1 required for the stable interaction with NEMO.

HOIP	NEMO A	NEMO B	Interaction
Arg377	-	Glu264	Electrostatic
Glu374	Lys270	-	Electrostatic
Arg375	-	Asp275	Electrostatic
Ala366	Gln259	-	Hydrogen bond
Val368	Leu267	Leu260	Hydrophobic
Pro376	-	Leu267, Val268	Hydrophobic
Leu369	Ala266	-	Hydrophobic

4. Conclusion

The overall study was conducted to understand the functional interactions of designed peptides that can be potentially used as drugs/therapeutics. The project uses an advanced approach to analyze peptide structure and molecular interactions based on NMR spectroscopy.

The cyclic antimicrobial peptides 8C and 9C featured a fixed backbone structure with the arranged distribution of charged and hydrophobic side chains. Their linear analogs, 8L and 9L, have a flexible backbone with the same amino acid sequence. The net positive charge of the peptides is important for the initial interaction with the negatively charged bacterial membrane. The initial stages of peptide-membrane interaction are the same for the cyclic and linear peptides; the peptide approaches the membrane surface and anchors on the surface through an extended network of electrostatic interaction and hydrogen bonds “waiting” for favorable conditions of the membrane bilayer. When favorable conditions, such as local lipid composition, lipid density, and accessibility of lipid hydrophobic clusters close to the membrane surface, are met, the aromatic side chains quickly penetrate the hydrophobic core region of the membrane.

However, the rate of peptide penetrating the membrane hydrophobic core depends on the peptide and/or the membrane's ability to adapt to each other's structure. When the peptide is flexible (as in the case of the linear peptides 8L and 9L), it can adapt to the membrane with minimal disturbance of the bilayer. Suppose a flexible peptide forms; a more stable oligomeric structure or the peptide backbone flexibility is restricted, as in the case of the cyclic peptides 8C and 9C. In that case, the membrane bilayer needs to adapt to the structure of the peptides. The adaptation of bilayer structure may involve forming lipid clusters or rafts, changes in bilayer curvature and thickness, and other processes that can affect membrane fluidity and integrity and destabilize the bilayer. Thus, our results show that the difference in structural adaptability explains the much higher antibacterial activity of the cyclic peptides studied in Aim 1.

Peptide HP2 was designed to mimic the region of HOIP NZF1 that interacts directly with the NEMO helical dimer. Analysis of the X-ray structure of the HOIP NZF1 – NEMO complex shows that the protein interaction requires extended surfaces, not just a set of point-to-point contacts of side chains. The NZF1 surface includes a hydrophobic “core” and several hydrophilic/electrostatic contacts to complement the NEMO surface composed of positively and negatively charged and hydrophilic and hydrophilic side chains. Recreating such a surface with a peptide requires that the peptide adopt a stable and well-defined conformation. Our results for the peptide HP2 show that the peptide cannot attain a stable conformation in solution. While a strong initial interaction with the target could force a flexible peptide to fold to the required conformation, NEMO and peptide HP2's molecular properties (such as charge and distribution of charged side chains) cannot establish a strong initial interaction.

Aim 1 and 2 results show that structural stability and structural localization of particular side chains are crucial for both peptide-membrane and peptide- or protein-protein interactions.

Our aim 2 confirms that the strength of the interaction between the proteins is often defined by the precise matching of the pre-formed interacting surfaces with minimal alignment. In contrast, aim 1 shows different mechanics of interaction where electrostatic interactions provide strong initial attraction. Then, the structures of the interacting partners (peptide and membrane in our case) may be adapted to carry out more extended interaction.

In the future, peptides 8C and 9C (Aim 1) could be considered as a lead for further development by fine-tuning the chemical properties of the side chains to boost the efficiency of interaction with bacterial targets while keeping low activity against mammalian cells, which would provide improved safety profile.

The results of Aim 2 demonstrate that replication of protein-protein interactions by peptides requires careful consideration of the peptide spatial structure with the required amino acid sequence. The design should consider the ability of the peptide to correctly fold and create the surface crucial for the peptide interaction with the target protein.

5. References

- Alanis, A. (2005). Resistance to Antibiotics: Are we in the post-antibiotic era? *Archives of medical research*, 697-705.
- Alderson, T. R., Lee, J. H., Charlier, C., Jinfa, Y., & Bax, A. (2017). The propensity for cis-proline formation in unfolded proteins. *Chembiochem*, 37-42.
- Amzel, M. L. (1998). Structure-based drug design. *Current Opinion in Biotechnology*, 366-369.
- Anderson, A. C. (2003). The Process of Structure-Based Drug Design. *Chemistry and Biology*, 787-797.
- Andrea Cavalli, X. S. (2007). *Proceedings of the National Academy of Sciences*. Washington, D.C: PNAs.
- Andrews, B. J., Dahesh, S., Davidson, A. R., & Marles, J. A. (2004). Protein-Protein Interaction Affinity Plays a Crucial Role in Controlling the Sho1p-Mediated Signal Transduction Pathway in Yeast. *Molecular Cell*, 813-823.
- Bahar, A. A., & Ren, D. (2013). Antimicrobial Peptides. *Pharmaceuticals*, 1543-1575.
- Brown, K., Park, S., Kanno, T., & Siebenlist, U. (1993). Mutual regulation of the transcriptional activator NF-kappa B and its inhibitor, I kappa B-alpha. *Proceedings of the national academy of sciences*, 2532-2536.
- Buer, B. C., Chugh, J., Al-Hshimi, H. M., & Marsh, N. G. (2010). Using Fluorine Nuclear Magnetic Resonance To Probe the Interaction of Membrane-Active Peptides with the Lipid Bilayer. *Biochemistry*, 5760-5765.
- Carneiro, M. G., AB, E., Theisgen, S., & Siegal, G. (2017). NMR in structure-based drug design. *Essays in Biochemistry*, 485-493.
- Cavanagh, J., Fairbrother, W. J., Palmer, III, A. G., Rance, M., & Skelton, N. J. (2007). *Protein NMR Spectroscopy: Principles and Practice Second Edition*. London: Elsevier Academic Press.
- Cheng, T., Li, Q., Zhou, Z., Wang, Y., & Bryant, S. H. (2012). Structure-Based Virtual Screening for Drug Discovery: A Problem-Centric Review. *The AAPS Journal*, 133-141.
- Chu, W.-M. (2013). Tumor necrosis factor. *Cancer Letters*, 222-225.
- Clore, G. M., Robien, M. A., & Gronenborn, A. M. (1993). Exploring the Limits of Precision and Accuracy of Protein Structures Determined by Nuclear Magnetic Resonance Spectroscopy. *Journal of Molecular Biology*, 82-102.

- Colman, P. M. (1994). Structure-based drug design. *Current Opinion Structural Biology*, 868-874.
- Cooper, B. M., Iegre, J., O'Donovan, D. H., Halvarsson, M. O., & Spring, D. R. (2020). Peptides as a platform for targeted therapeutics for cancer: peptide-drug conjugates. *Chemical Society Reviews*, 50.
- Deber, C. M., & Stone, T. A. (2017). Therapeutic design of peptide modulators of protein-protein interactions in membranes. *Biochimica et biophysica acta - biomembranes*, 577-585.
- Doost, A. S., Akbari, M., Stevens, C. V., Seriwati, A. D., & Meeren, V. P. (2019). A review on nuclear overhauser enhancement (NOE) and rotating-frame overhauser effect (ROE) NMR techniques in food science: Basic principles and applications. *Trends in Food Science and Technology*, 16-24.
- Eisenmesser, E. Z., Millet, O., Labeikovsky, W. K.-W., Bosco, D. A., Skalicky, J. J., Kay, L. E., & Kern, D. (2005). Intrinsic dynamics of an enzyme underlie catalysis. *Nature*, 117-121.
- Emwas, A.-H., Merzaban, J. S., & Serrai, H. (2015). Theory and Applications of NMR-Based Metabolomics in Human Disease Diagnosis. *Application of NMR Spectroscopy*, 93-130.
- Esteban-Martin, S., Fenwick, R. B., & Salvatella, X. (2012). Synergistic use of NMR and MD simulations to study the structural heterogeneity of proteins. *WIREs Comput Mol Sci*, 466-478.
- Fosgerau, K., & Hoffmann, T. (2014). Peptide Therapeutics: Current status and future directions. *Drug Discovery Today*, 20.
- Giralt, E., & Nevola, L. (2015). Modulating Protein-Protein interactions: the potential of peptides. *Chemical Communications*, 51.
- Guntert, P. (2004). Automated NMR Structure Calculation With CYANA. *Protein NMR Techniques*, 353-378.
- Guntert, P. (2008). Automated Structure Determination from NMR Spectra. *European Biophysics Journal*, 129.
- Gustafson, C. L., Parsley, N. C., Asimgil, H., Lee, H.-W., Ahlback, C., Michael, A. K., . . . Partch, C. L. (2017). A slow conformational switch in the BMAL1 transactivation domain modulates circadian rhythms. *Mol Cell*, 447-457.
- Haas, T. L., Emmerich, C. H., Gerlach, B., Schmukle, A. C., Cordier, S. M., Rieser, E., . . . Walczak, H. (2009). Recruitment of the Linear Ubiquitin Chain Assembly Complex Stabilizes the TNF-R1 Signaling Complex and Is Required for TNF-Mediated Gene Induction. *Molecular Cell*, 831-844.
- Hancock, R. E., & Sahl, H.-G. (2006). Antimicrobial and host-defense peptides as new anti-infective therapeutic strategies. *Nature Biotechnology*, 1551-1557.

- Hiroaki Fujita, S. R. (2014 Apr). Mechanism underlying I κ B kinase activation mediated by the linear ubiquitin chain assembly complex. *Mol Cell Biol.*, 34(7):1322-35. doi:10.1128/MCB.01538-13
- Israel, A. (2010). The IKK complex a central regulator of NF-kappaB activation. *Cold Spring Harbor perspectives in biology*.
- Izadpanah, A., & Gallo, R. L. (2005). Antimicrobial peptides. *J Am Acad Dermatol.*, 381-390.
- Kaspar, A. A., & Reichert, J. M. (2013). Future directions for peptide therapeutics development. *Drug Discovery Today*, 807-817.
- Keller, R. (1996). *The Computer-Aided Resonance Assignment Tutorial*. Zurich, Switzerland: Cantina Verlag.
- Kleckner, I. R., & Foster, M. P. (2012). An introduction to NMR-based approaches for measuring protein dynamics. *Biochim Biophys Acta*, 942-68.
- Koczulla, A. R., & Bals, R. (2012). Antimicrobial Peptides. *Drugs*, 389-406.
- Li, J., Koh, J.-J., Liu, S., Lakshminarayanan, R., Verma, C. S., & Beuerman, R. W. (2017). Membrane Active Antimicrobial Peptides: Translating Mechanistic Insights to Design. *Frontiers in Neuroscience*, 11:73.
- Li, L., Vorobyov, I., & Allen, T. W. (2013). The Different Interactions of Lysine and Arginine Side Chains with Lipid Membranes. *The Journal of Physical Chemistry B*, 11906-11920.
- Li, X.-H., Fang, X., & Gaynor, R. B. (2001). Role of IKK γ /NEMO in Assembly of the I κ B Kinase Complex. *Journal of Biological Chemistry*, 4494-4500.
- Lipinski, C. A., Lombardo, F., Dominy, B. W., & Feeney, P. J. (2001). Experimental and computational approaches to estimate solubility and permeability in drug discovery and development settings. *Advanced Drug Delivery Reviews*, 3-26.
- Lohan, S., Mandal, D., Choi, W., Konshina, A. G., Tiwari, R. K., Efremov, R. G., . . . Parang, K. (2022). Small Amphiphilic Peptides: Activity Against Broad Range of Drug-Resistant. *Journal of Medicinal Chemistry*, 665-687.
- Mandal, S., Moudgil, M., & Mandal, S. K. (2009). Rational drug design. *European Journal of Pharmacology*, 90-100.
- Maroti, G., Kereszt, A., Kondorosi, E., & Mergaert, P. (2011). Natural roles of antimicrobial peptides in microbes, plants, and animals. *Research in Microbiology*, 363-374.
- Maslennikov, I. V., Sobol, A. G., Gladky, K. V., Lugovskoy, A. A., Ostrovsky, A. G., Tsetlin, V. I., . . . Arseniev, A. S. (1998). Two distinct structures of a-conotoxin GI in aqueous solution. *Eur. J. Biochem*, 238-247.

- Mavromoustakos, T., Durdagi, S., Koukoulitsa, C., Simcic, M., Papadopoulos, M. G., Hodoscek, M., & Gradadolnik, G. S. (2011). Strategies in the rational drug design. *Current Medicinal Chemistry*, 2517-2530.
- McGowan Jr, J. E., & Tenover, F. C. (1996). Reasons for the Emergence of Antibiotic Resistance. *The American Journal of the Medical Sciences*, 9-16.
- Mitchell, N., Seaton, P., & Pokorny, A. (2016). Branched phospholipids render lipid vesicles more susceptible to membrane-active peptides. *Biochimica et Biophysica Acta (BBA) - Biomembranes*, 988-994.
- Mittermaier, A. K., & Kay, L. E. (2009). Observing biological dynamics at atomic resolution using NMR. *Trends in Biochemical Sciences*, 601-611.
- Niu, J., Shi, Y., Iwai, K., & Wu, Z.-H. (2011). LUBAC regulates NF- κ B activation upon genotoxic stress by promoting linear ubiquitination of NEMO. *The EMBO Journal*, 3741-3753.
- Oh, D., Sun, J., Shirazi, A. N., LaPlante, K. L., Rowley, D. C., & Parang, K. (2014). Antibacterial Activities of Amphiphilic Cyclic Cell-penetrating Peptides against Multidrug-Resistant Pathogens. *Molecular Pharmaceutics*, 3528-3536.
- Pastor, A., & Martinez-Viviente, E. (2008). NMR spectroscopy in coordination supramolecular chemistry: A unique and powerful methodology. *Coordination Chemistry Reviews*, 2314-2345.
- Pettersen EF, G. T. (2004). UCSF Chimera--a visualization system for exploratory research and analysis. San Francisco, California, USA: University of California, San Francisco.
- Pollastri, M. P. (2010). Overview of the Rule of Five. *Current Protocol Pharmacology*.
- Rahighi, S., Ikeda, F., Kawasaki, M., Akutsu, M., Suzuki, N., Kato, R., . . . Dikic, I. (2009). Specific Recognition of Linear Ubiquitin Chains by NEMO is Important for NF- κ B activation. *Cell Press*, 1098-1109.
- Riahifar, N., S., M., Aldakhil, T., Nunez, F., Alshammari, Q., Alshammari, S., . . . Tiwari, R. K. (2018). Design, of synthesized and evaluated amphiphilic cyclic and linear peptides composed of hydrophobic and positively-charged amino acids as antibacterial agents. *Molecules*, 23, 2722.
- Roff, M., Thompson, J., Rodriguez, M. S., Jacque, J. M., Baleux, F., Arenzana-Seisdedos, F., & Hay, R. T. (1996). Role of IkappaBalpha ubiquitination in signal-induced activation of NF-kappaB in vivo. *Journal of Biological Chemistry*, 7844-7850.
- Sarkar, S. K., E, Y. P., Sullivan, C. E., & Torchia, D. A. (1984). Detection of cis and trans-X-Pro peptide bonds in proteins by ^{13}C NMR: application to collagen. *Proc Natl Acad Sci U S A*, 4800-4803.

- Sautrey, G., El Khoury, M., Giro dos Santos, A., Lins, L., Decout, J.-L., & Mingeot-Leclercq, M.-P. (2015). Negatively Charged Lipids as a Potential Target for New Amphiphilic Aminoglycoside Antibiotics. *Journal of Biological Chemistry*, P13864-13874.
- Sivagami, G., & Srinivasan, M. (2018). Mechanism of NF- κ B p65 and strategies for therapeutic manipulation. *Journal of Inflammation Research*, 407-419.
- Soltész, D., Szabó, I., & Bánóczy, Z. (2023). The Balance between Hydrophobicity/Aromaticity and Positively Charged Residues May Influence the Cell Penetration Ability. *Pharmaceutics*, 1267.
- Szantay, C. (2015). The Human Aspects of Scientific Thinking in NMR Spectroscopy and Mass Spectrometry. *Anthropic Awareness*.
- Tan, S., & Tatsumura, Y. (2015). Alexander Fleming (1881-1955): Discoverer of penicillin. *Singapore Med J*, 366-367.
- Tokunaga, F., Nakagawa, T., Nakahara, M., Saeki, Y., Taniguchi, M., Sakata, S.-i., . . . Iwai, K. (2011). SHARPIN is a component of the NF- κ B-activating linear ubiquitin chain assembly complex. *Nature*, 633-636.
- Vincendeau, M., Hadian, K., Messias, A. C., Brenke, J. K., Halander, J., Griesbach, R., . . . Sattler, M. (2016). Inhibition of Canonical NF- κ B Signaling by a Small Molecule Targeting NEMO-Ubiquitinating Interaction. *Nature Scientific Reports*.
- Wajant, H., Pfizenmaier, K., & Scheurich, P. (2003). Tumor necrosis factor signaling. *Cell Death and Differentiation*, 45-65.
- Wen, J.-L., Xue, B.-L., Xu, F., & Sun, R.-C. (2012). Unveiling the Structural Heterogeneity of Bamboo Lignin by In Situ HSQC NMR Technique. *Bioenerg. Res.*, 886-903.
- Wuthrich, K. (1986). *NMR of Proteins and Nucleic Acids*. Zurich, Switzerland: John Wiley & Sons.